JOURNAL OF GEOPHYSICAL RESEARCH, VOL. 114, G02006, doi:10.1029/2008JG000728, 2009

Spatially explicit simulation of hydrologically controlled carbon and nitrogen cycles and associated feedback mechanisms in a boreal ecosystem

Ajit Govind,[1] Jing Ming Chen,[1] and Weimin Ju[2]

Received 12 March 2008; revised 10 September 2008; accepted 2 October 2008; published 21 April 2009.

[1] Ecosystem models that simulate biogeochemical processes usually ignore hydrological controls that govern them. It is quite possible that topographically driven water fluxes significantly influence the spatial distribution of C sources and sinks because of their large contribution to the local water balance. To investigate this, we simulated biogeochemical processes along with the associated feedback mechanisms in a boreal ecosystem using a spatially explicit hydroecological model, boreal ecosystem productivity simulator (BEPS)−TerrainLab V2.0, that has a tight coupling of ecophysiological, hydrological, and biogeochemical processes. First, the simulated dynamics of snowpack, soil temperature, net ecosystem productivity (NEP), and total ecosystem respiration (TER) were validated with high-frequency measurements for 2 years. The model was able to explain 80% of the variability in NEP and 84% of the variability in TER. Further, we investigated the influence of topographically driven subsurface base flow on soil C and N cycling and on the spatiotemporal patterns of C sources and sinks using three hydrological modeling scenarios that differed in hydrological conceptualizations. In general, the scenarios that had nonexplicit hydrological representation overestimated NEP, as opposed to the scenario that had an explicit (realistic) representation. The key processes controlling the NEP differences were attributed to the combined effects of variations in photosynthesis (due to changes in stomatal conductance and nitrogen (N) availability), heterotrophic respiration, and autotrophic respiration, all of which occur simultaneously affecting NEP. Feedback relationships were also found to exacerbate the differences. We identified six types of NEP differences (biases), of which the most commonly found was due to an underestimation of the existing C sources, highlighting the vulnerability of regional-scale ecosystem models that ignore hydrological processes.

Citation: Govind, A., J. M. Chen, and W. Ju (2009), Spatially explicit simulation of hydrologically controlled carbon and nitrogen cycles and associated feedback mechanisms in a boreal ecosystem, *J. Geophys. Res.*, *114*, G02006, doi:10.1029/2008JG000728.

1. Introduction

[2] The terrestrial C cycle is closely linked to climatic, hydrological, and nutrient controls on vegetation [*Porporato et al.*, 2003]. Interactions between ecosystem processes at different spatiotemporal scales vary nonlinearly creating uncertainties in the terrestrial C cycle [*Post et al.*, 1992]. Of these, hydrological controls are likely to be the most dominant and least explored because they are multifaceted and range widely in the form of plant water stress (excess or deficit), effects on total ecosystem respiration (TER), methane production, transport of dissolved organic C (DOC), snow-mediated thermal insulation, evapotranspiration (ET), soil chemical changes, and nutrient mineralizations, etc., to name a few. Hydrological controls on biogeochemical cycles and their implications on climate change have recently gained recognition [e.g., *Gedney et al.*, 2006; *Betts et al.*, 2007]. Since the early 1990s, there has been an increased interest in the measurement of fluxes of mass and energy within the biosphere (e.g., the Long-Term Ecological Network) and also at the biosphere-atmosphere interface (e.g., Fluxnet) [*Baldocchi*, 2008]. In many of these studies, hydrologically controlled primary production [*Amiro et al.*, 2006; *Humphreys et al.*, 2006], ET [*Zhang et al.*, 2007; *Beringer et al.*, 2005], nitrogen cycling [*Traore et al.*, 2007; *Piirainen et al.*, 2007; *Ford et al.*, 2007], DOC export [*Fraser et al.*, 2001; *Aitkenhead-Peterson et al.*, 2007], methane production [*Blodau et al.*, 2007; *Zhuang et al.*, 2004], and carbon sequestration [*Byrne et al.*, 2007; *Dragoni et al.*, 2007] processes have been documented in various ecosystems.

[3] Recently, modeling of the coupled C and water cycles has become an indispensable approach in ecosystem research. This is because modeling helps to articulate the underlying biophysical processes and is also an efficient

---

[1] Department of Geography, University of Toronto, Toronto, Ontario, Canada.

[2] International Institute for Earth System Sciences, Nanjing University, Nanjing, China.

0148-0227/09/2008JG000728$09.00

approach to scale various processes across a wide spectrum of spatial and temporal scales. To date, modeling of coupled water and biogeochemical cycles is being conducted at point scale [*Grant et al.*, 2006; *Ju et al.*, 2006; *Rodriguez-Iturbe et al.*, 2001; *Porporato et al.*, 2003; *Daly et al.*, 2004;], watershed scale [*Mackay and Band*, 1997; *Tague and Band*, 2004; *Band et al.*, 2001; *Chen et al.*, 2005], regional scales [*Liu et al.*, 1997; *Potter et al.*, 2001; *Coops et al.*, 2007; *Ju and Chen*, 2005], and global scales [*Hunt et al.*, 1996; *Nemani et al.*, 2003; *Potter et al.*, 2003; *White et al.*, 2005; *Zhao et al.*, 2005]. These studies differ widely in their sophistications, complexities, temporal resolutions (half-hourly to annual), and temporal spans (hourly to decadal). Most of the modeling studies have been using ecological indicators such as biomass [*Ju and Chen*, 2005]; gross primary productivity (GPP) [*Frolking et al.*, 1996; *Wang et al.*, 2001]; net primary productivity (NPP) [*Ju and Chen*, 2005; *Zhou et al.*, 2006]; ecosystem respiration [*Mcguire et al.*, 2000; *Reichstein et al.*, 2003; *Ito et al.*, 2007]; N fluxes [*Creed and Band*, 1998; *Arain et al.*, 2006]; leaf area index (LAI) [*Band et al.*, 1993; *Kergoat*, 1998]; DOC fluxes [*Neff and Asner*, 2001; Hornberger et al. 1994]; water use efficiency [*Yu et al.*, 2004; *Winner et al.*, 2004; *Utset et al.*, 2004], etc., to demonstrate the hydrological effects on terrestrial C or biogeochemical cycles. Moreover, researchers have been employing either ecohydrological [e.g., *Schulze et al.*, 1995] or hydroecological approaches [e.g., *Tague and Band*, 2004; *Chen et al.*, 2005], and hence, models greatly differ in the manner in which the hydrological influences on C cycle are represented. In a recent intercomparison study, it was shown by *Morales et al.* [2005] that most of the ecosystem models inadequately simulated ecosystem processes because of the incompleteness in the representations of hydroecological processes.

[4] Interactions between water and biogeochemical cycles cannot be fully explained using indicators that are only part of the C balance (e.g., GPP, NPP, TER, DOC, etc.). A spatially explicit simulation of net ecosystem productivity (NEP) is warranted to fully understand the connections between hydrological and biogeochemical cycles. Although many point-scale models have detailed descriptions of ecosystem processes, only a few studies demonstrate the spatiotemporal distribution of NEP [e.g., *Turner et al.*, 2006; *Potter*, 1997; *Ju and Chen*, 2005]. This is because the dynamics of NEP is complicated and is controlled by several subcomponent processes that are closely related with feedback relationships making the system highly nonlinear. In an ideal modeling domain, primary production and biogeochemical processes should be modeled with a tight coupling between environmental and edaphic controls as a function of soil hydrothermal fluctuations in order to fully understand the terrestrial C cycle [*Arain et al.*, 2006]. Incorporation of explicit hydrological representations in conjunction to ecological processes is an essential requirement to achieve realistic simulations of biogeochemical processes in terrestrial ecosystems.

[5] Local-scale hydrological regimes are controlled by landscape-scale hydrological processes because of the topographic differences on the Earth's surface or subsurface [*Dietrich and Perron*, 2006]. Hence, point-scale models cannot comprehensively represent hydrological regimes because they abstract lateral hydrological processes. Currently, an integrated approach representing a complete description of the hydrological cycle is not often adopted in most of the ecological models [*Kuchment et al.*, 2006]. Studies conducted by *Govind et al.* [2006], *Sonnentag et al.* [2008], and A. Govind et al. (Effect of lateral hydrological processes on photosynthesis and evapotranspiration in a boreal ecosystem, submitted to *Ecohydrology*, 2009) demonstrate that lateral subsurface base flow could significantly alter local-scale water balance and hence, the spatial distribution of GPP and ET. Although these attempts demonstrate only a first-order interaction between water and C cycles, there is much speculation about the hydrologically controlled biogeochemical processes. Because topographic effects on lateral hydrological processes are not often explicitly represented in regional-scale ecosystem models [*Grant*, 2004], it is quite probable that these models are likely to have several types of systematic bias in their NEP estimates.

[6] Studies have demonstrated that high-latitude boreal forests are terrestrial C sinks [*Thompson et al.*, 1996; *Chen et al.*, 2003]. However, this C cycling pattern is quite variable in space and time. In order to investigate the hydrological effects on C and N cycling and the associated feedback relationships in boreal ecosystems, we developed a hydroecological model, boreal ecosystem productivity simulator (BEPS)−TerrainLab V2.0 [*Govind et al.*, 2009] that has a tighter coupling of ecophysiological, hydrological, and biogeochemical processes in a spatially explicit manner. In this paper, we introduce various biogeochemical conceptualizations in BEPS-TerrainLab V2.0 and test its ability to simulate various processes using high-frequency measurements in a boreal ecosystem in eastern Canada. Furthermore, we investigate the influence of lateral hydrological processes on the spatial distribution of NEP using a numerical experiment employing modeling scenarios that represent different hydrological representations that are commonly found in many ecological models.

2. Model Description

[7] BEPS-TerrainLab V2.0 originated from the boreal ecosystem productivity simulator (BEPS) [*Liu et al.*, 1997] developed during the boreal ecosystem-atmosphere study (BOREAS). BEPS-TerrainLab V1.0 [*Govind et al.*, 2006; *Chen et al.*, 2007; *Sonnentag et al.*, 2008] was an improvement over BEPS with the inclusion of a distributed hydrological model, TerrainLab [*Chen et al.*, 2005]. BEPS-TerrainLab V2.0 can be described as a hydroecological model that simulates the coupled hydrological, ecophysiological, and biogeochemical processes and the associated feedback mechanisms in a spatially explicit and tightly linked manner. A complete description of the hydrological and ecophysiological processes within BEPS-TerrainLab V2.0 can be found in the work of *Govind et al.* [2009]. This model runs at a daily time step and the modeling period is generally 1 or 2 years.

[8] Daily canopy-scale photosynthesis (as GPP) is modeled using a leaf-level, instantaneous model [*Farquhar et al.*, 1980] employing a spatial and temporal upscaling strategy [*Chen et al.*, 1999]. A Penman-Monteith formulation is used to calculate leaf-scale or point-scale ET. Spatial

upscaling of leaf-level ecophysiological processes (GPP and ET) is carried out using a four-leaf scheme that uses fractions of LAI as weighting factors that correspond to different leaf physiological statuses within a canopy. Environmental controls (net radiation, stomatal conductance, etc.) specific to different radiation and soil water regimes are used to simulate leaf-level ET and GPP for multilayer canopies (overstory, understory, and moss layer).

[9] In order to realistically represent hydrological regimes within each modeling unit (pixel), a water balance equation is solved in a spatially explicit manner having interpixel connectivity using surface and subsurface lateral water fluxes that are topographically driven. Solving this detailed water balance equation having landscape-scale hydrological processes as subcomponents adequately represents the local-scale hydrological regimes. Details on the C and N dynamics as a function of hydrothermal processes are the focus of this paper. In the current model setup, we assume DOC or methane fluxes are negligible. Thus, NEP is the difference between GPP and TER.

2.1. Carbon Cycling Processes Within BEPS-TerrainLab V2.0

2.1.1. Autotrophic Respiration

[10] On a daily basis, a part of the C assimilated in the form of photosynthesis (details given in Appendix A) is used for growth respiration (R_g) and maintenance respiration (R_m), together known as autotrophic respiration (R_a). Various components of the vegetation (leaf, stem, and root) at various levels (overstory, understory, and moss) have R_a losses. In BEPS-TerrainLab V2.0, R_g is assumed to be 25% of GPP for all the land cover types [*Chen et al.*, 1999; *Liu et al.*, 1999; *Ju et al.*, 2006]. R_m is temperature-dependent and is contributed to by leaf, stem, and root. Total R_m of a pixel is modeled as

$$R_m = \sum_{j=1}^{3}\sum_{i=1}^{4} R_{m,i} = \sum_{j=1}^{3}\sum_{i=1}^{4} M_i . r_{m,i} . Q_{10}^{\frac{(T-T_b)}{10}} \tag{1}$$

Here i refers to different plant parts such as leaf, stem, coarse root, or fine root, and j refers to the canopy layer, i.e., overstory, understory, or the moss layer; M is the C pool size associated with a biomass type, i; $r_{m,i}$ is a biomass C-pool-specific respiration rate at a base temperature T_b (27°C); and T is assumed to be the ambient air temperature for leaves and stems whereas it is soil temperature for fine roots and coarse roots. The remainder of the C after accounting for R_a is NPP (gC m^{-2} d^{-1}) which is further partitioned into leaf, wood, coarse root, and fine root biomass C pools.

2.1.2. Heterotrophic Respiration

[11] Heterotrophic respiration (R_h) is comprehensively calculated in a manner similar to the CENTURY model [*Parton et al.*, 1987] with several modifications as suggested by *Ju and Chen* [2005] and *Ju et al.* [2007]. The soil C cycle in BEPS-TerrainLab V2.0 runs at a daily time step. The soil C dynamics is conceptualized on the basis of the dynamics of various C pools that decompose either to free CO_2 or interchange between the soil C pools. Unlike the CENTURY model, which was originally developed for grasslands or agroecosystems, a greater number of biomass and litter pools are conceptualized in BEPS-TerrainLab V2.0 in order to adequately simulate the boreal forest C cycle. Biomass C pools demarcated explicitly as wood (C_w), foliage (C_l), coarse root (C_{cr}) and fine root (C_{fr}) C pools decompose to nine soil C pools (five litter and four soil C pools), i.e., (1) surface structural litter C pool, C_{ssd}, (2) soil structural litter C pool, C_{fsd}, (3) coarse woody litter C pool, C_{cd}, (4) surface metabolic litter C pool, C_{smd}, (5) soil metabolic litter C pool, C_{fmd}, (6) surface microbial C pool, C_{sm}, (7) soil microbial C pool, C_m, (8) slow C pool, C_s, and (9) passive C pool, C_p. Coarse woody litter C pool, C_{cd}, is a new addition in BEPS-TerrainLab V2.0 to account for the dead wood component in the forest C cycle. On the basis of various factors such as soil moisture, soil temperature, decomposition rates, the quantities (sizes) and qualities (C:N ratios), C pools are updated on a daily basis. Total R_h is the sum of C released to the atmosphere as CO_2 from all the soil C pools during their decomposition as shown below.

$$R_{h_i} = \sum_{j=1}^{9} k_{j_i} . C_{j_i} \tag{2}$$

where R_{h_i} is the total heterotrophic respiration on day i, k_{j_i} (d^{-1}) is the rate of C decomposed from the jth soil C pool on the ith day, and C_{j_i} is the size of the jth C pool on the ith day. The actual decomposition rates (k_j) are determined by constraining a C-pool-specific maximum decomposition rate (K_j) using scalars that correspond to abiotic factors as summarized below.

$$k_{j_i} = \begin{cases} K_j \xi_{j_i} A_i L_j & j = Pools - 1, 2, 3 \\ K_j \xi_{j_i} A_i & j = Pools - 4, 5, 8, 9 \\ K_j A_i \eta & j = Pool - 7 \\ K_j A_i L_j & j = Pool - 6 \end{cases} \tag{3}$$

[12] In the above equation, K_j is a land-cover-specific parameter (see Table 1). A daily scheme is implemented in BEPS-TerrainLab V2.0 using the temporally downscaled maximum decomposition coefficients from *Chen et al.* [2003], i.e., $K_{\text{daily}} = K_{\text{annual}}/365$. However, the actual decomposition rates (k_j) are calculated according to equation (3) using scalars that correspond to daily variations in abiotic factors that are simulated in a process-based manner. This is sufficient to capture the biogeochemical processes at daily time steps. These scalars include A_i, the combined effects of soil temperature and moisture; η, the effect of soil texture on soil microbial turnover; L, the effect of lignin content for structural litter decomposition; and ξ, the effect of N availability on C pool decomposition. A_i is calculated as the product of soil moisture (M_{s_i}) and soil temperature (T_{m_i}) scalars:

$$A_i = M_{s_i} \times T_{m_i} \tag{4}$$

[13] The soil moisture effect, M_{si}, is calculated as a function of volumetric soil moisture content (VSMC, θ) as shown below [*Potter*, 1997; *Ju et al.*, 2006, 2007]:

$$M_{s_i} = 5.44\left[\frac{\theta_i}{\theta_s}\right] - 5.03\left[\frac{\theta_i}{\theta_s}\right]^2 - 0.472 \tag{5}$$

Table 1. Land-Cover-Specific Parameters Used for Biogeochemical Modeling Within BEPS-TerrainLab V2.0[a]

Parameters	Unit	Conifers	Mixed	Deciduous	Wetlands	Reference
Leaf maintenance respiration coefficient	–	2×10^{-3}	2×10^{-3}	2×10^{-3}	2×10^{-3}	1
Stem maintenance respiration coefficient	–	1×10^{-3}	1×10^{-3}	1×10^{-3}	1×10^{-3}	1
Coarse root maintenance respiration coefficient	–	1×10^{-3}	1×10^{-3}	1×10^{-3}	1×10^{-3}	1
Fine root maintenance respiration coefficient	–	2×10^{-3}	2×10^{-3}	2×10^{-3}	2×10^{-3}	1
Atmospheric nitrogen deposition	gN m^{-2} d^{-1}	8.2×10^{-4}	8.2×10^{-4}	$8.2\text{x}10^{-4}$	8.2×10^{-4}	2
Wood turnover rate	gC m^{-2} d^{-1}	7.64×10^{-5}	7.64×10^{-5}	7.89×10^{-5}	1.97×10^{-5}	2
Leaf turnover rate	gC m^{-2} d^{-1}	7.37×10^{-5}	7.34×10^{-5}	1.23×10^{-4}	3.07×10^{-5}	2
Coarse root turnover rate	gC m^{-2} d^{-1}	5.27×10^{-4}	1.08×10^{-3}	2.74×10^{-3}	6.85×10^{-4}	2
Fine root turnover rate	gC m^{-2} d^{-1}	1.63×10^{-3}	1.63×10^{-3}	1.63×10^{-3}	4.07×10^{-4}	2
Surface structural litter decomposition rate	gC m^{-2} d^{-1}	$(3.9LA\xi)/365$				3
Surface metabolic litter decomposition rate	gC m^{-2} d^{-1}	$(14.8A\xi)/365$				3
Soil structural litter decomposition rate	gC m^{-2} d^{-1}	$(4.8LA\xi)/365$				3
Soil metabolic litter decomposition rate	gC m^{-2} d^{-1}	$(18.5A\xi)/365$				3
Coarse woody litter decomposition rate	gC m^{-2} d^{-1}	$(2.88LA\xi)/365$				3
Surface microbial decomposition rate	gC m^{-2} d^{-1}	$(6.0LA)/365$				3
Soil microbial decomposition rate	gC m^{-2} d^{-1}	$(7.3A\eta)/365$				3
Slow carbon decomposition rate	gC m^{-2} d^{-1}	$(0.2A\xi)/365$				3
Passive carbon decomposition rate	gC m^{-2} d^{-1}	$(0.0045A\xi)/365$				3
NPP allocation coefficient to wood	–	0.3010	0.3817	0.4624	0.4624	2
NPP allocation coefficient to leaf	–	0.2128	0.2077	0.2226	0.2226	2
NPP allocation coefficient to coarse root	–	0.1483	0.1536	0.1190	0.1190	2
NPP allocation coefficient to fine root	–	0.3479	0.2570	0.1960	0.1960	2

[a] Reference numbers are as follows: 1, *Chen et al.* [1999]. 2, Coefficients from *Chen et al.* [2003] are divided by 365 for daily applications; the coefficients for wetlands are assumed to be ~0.5 times the values for open lands given by *Chen et al.* [2003]. 3, See Govind et al. (manuscript in revision, 2009) for a detailed description of the fates of individual pool decompositions. A is a factor that represents the influence of soil temperature and soil moisture in a combined manner (equation (4)), ξ is the effect of N availability on C pool decomposition, L is the effect of lignin fraction, and η is the effect of soil texture.

In the above equation, M_{s_i} is assumed to range between 0 and 1 even if the values fall below 0 at extreme values of θ_i. Here θ_i is the outcome of the detailed local-scale water balance that is solved in a spatially explicit manner [*Govind et al.*, 2009]. Most of the hydroecological processes are considered in the water balance, including the lateral water fluxes that contribute or distribute water from neighboring pixels to a pixel in consideration, thus ensuring that landscape-scale hydrological processes affect local-scale water balance.

[14] The soil temperature effect T_{m_i} is described as shown below [*Lloyd and Taylor*, 1994; *Chen et al.*, 2003]:

$$T_{m_i} = e^{308.56.\left[\left(\frac{1}{35+46.02}\right)-\left(\frac{1}{Ts_i+46.02}\right)\right]} \tag{6}$$

In equation (6), Ts_i is the soil temperature, which plays a critical role in determining the rate of decomposition of various soil C pools. The nature of M_{s_i} and Ts_i is shown in Figure 1.

[15] Since soil temperature is a critical parameter for simulating biogeochemical processes, in BEPS-TerrainLab V2.0, Ts_i is calculated using the Fourier one-dimensional heat transfer equation for a six-layered profile (one dynamic snow layer and five soil layers) as shown below:

$$C_i \frac{\partial Ts}{\partial t} = \lambda_i \frac{\partial^2 Ts}{\partial d^2} \tag{7}$$

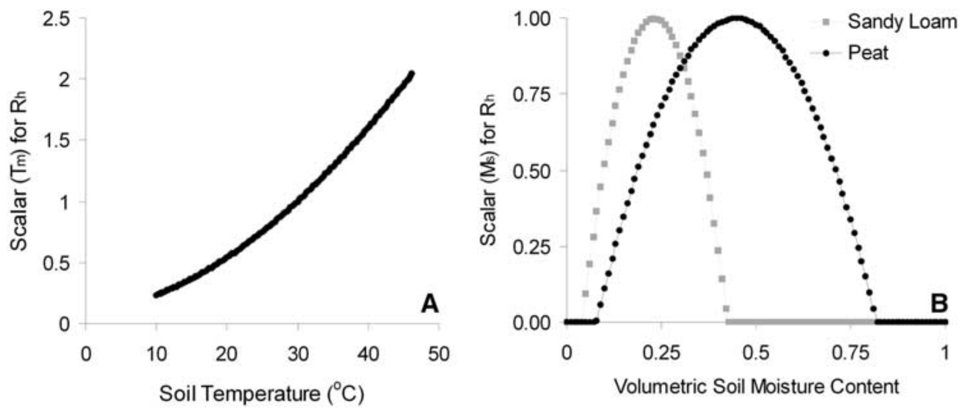

Figure 1. (a) Nature of soil temperature scalar for heterotrophic respiration and (b) soil moisture scalar for heterotrophic respiration.

Since equation (7) is variable in space, time, and depth and is parabolic in nature, it can be numerically solved employing the Crank-Nicholson scheme, as shown below:

$$\frac{C_i d_i \left[Ts_{i,t+1} - Ts_{i,t}\right]}{\Delta t} = 2(1-f)\left[\frac{Ts_{i-1,t} - Ts_{i,t}}{\frac{d_{i-1}}{\lambda_{i-1}} + \frac{d_i}{\lambda_i}} - \frac{Ts_{i,t} - Ts_{i,t+1}}{\frac{d_i}{\lambda_i} + \frac{d_{i+1}}{\lambda_{i+1}}}\right] + f\left[\frac{Ts_{i-1,t+1} - Ts_{i,t+1}}{\frac{d_{i-1}}{\lambda_{i-1}} + \frac{d_i}{\lambda_i}} - \frac{Ts_{i,t+1} - Ts_{i,t+1}}{\frac{d_i}{\lambda_i} + \frac{d_{i+1}}{\lambda_{i+1}}}\right] \tag{8}$$

In equation (8), C_i is the volumetric soil heat capacity ($Jm^{-3}°C^{-1}$), λ is the thermal conductivity ($\mathrm{Wm^{-1}\ C^{-1}}$), d is the vertical depth of a layer i, t is the time step, and f is the weight given to the semi-implicit formulation ($f = 0.5$). Snow depth plays an important role in determining the wintertime Ts_i in boreal ecosystems. Snow depth is modeled by temporally varying the snow density and snow water equivalent as affected by snowmelt (radiation melt or temperature melt) and snow sublimation.

[16] On a daily basis, a small fraction of C is lost (decomposed) or added (from other C pools) which together alter the size of a given soil C pool x as shown below:

$$Cx_i = Cx_{i-1} + \Delta Cx_i \tag{9}$$

where Cx_{i-1} is the size of the C pool x on the previous day, $i - 1$. ΔCx_i is the change in the pool x on a daily basis calculated assuming first-order kinetics [*Paul and Clark*, 1996]. The procedure to calculate ΔCx_i for each soil C pool is different and depends on various environmental factors. The equations for calculating ΔCx_i are shown in Appendix A. This scheme, however, requires the proper initialization of various C pools before the actual simulation. For the first day, Cx_{i-1} for a given C pool is the value obtained from a spin-up procedure using a long-term C balance model (InTEC) [*Chen et al.*, 2000] considering the effects of climate change, CO_2 fertilization, N deposition, and disturbance (A. Govind et al., Modeling the long-term carbon balance of a boreal ecosystem under climate change, CO_2 fertilization, nitrogen deposition, and disturbance effects., under revision for *Geoderma*, 2009; hereinafter referred to as Govind et al., manuscript in revision, 2009).

2.2. Soil Nitrogen Cycle Within BEPS-TerrainLab V2.0

[17] Availability of soil N to plants is determined by three processes as shown below:

$$N_{avail} = N_{dep} + N_{fix} + N_{\min} \tag{10}$$

where N_{dep} is dry and wet deposition of N from the atmosphere; N_{fix} is the biological N fixation by microorganisms present in the rhizosphere; and $N_{\min}$ is the net N mineralization which results from the decomposition of soil C pools as a function of abiotic factors. N_{fix} (atmospheric and biological combined) is empirically calculated as a function of daily precipitation and the sizes of the microbial C pools, C_{sm} and C_m, analogous to *Ju et al.* [2007], after adjusting for daily calculations.

$$N_{fix_i} = \left[\frac{c1 \times 2.0^{\frac{Ts_i}{10}} \times P_i}{0.45}\right] \times \left(\frac{C_{sm_i} + C_{m_i}}{200}\right) \tag{11}$$

In equation (11), N_{fix_i} is the N fixation in $\mathrm{gN\ m^{-2}\ d^{-1}}$. The coefficient $c1$ is the daily N fixation rate. T_{s_i} is the daily mean soil temperature, P_i is daily precipitation (in meters), and C_{sm_i} and C_{m_i} are the sizes of surface and soil microbial C pools, respectively, on the day, i.

[18] In BEPS-TerrainLab V2.0, N mineralization is conceptualized similar to *Ju et al.* [2007]. N mineralization and/or N immobilization could occur as a function of the dynamics of soil C pool sizes and their C:N ratios. If the net effect is N mineralization, it contributes to the total available N in the soil (other components being N_{dep} and N_{fix} as shown in equation (10)). From the available soil N, plant N uptake is calculated as a function of root biomass and ambient hydrothermal conditions. N uptake affects leaf N which increases the maximum carboxylation rate, Vcmax, an important parameter for photosynthesis. Increase in Vcmax affects photosynthesis which leads to C increase within the biomass and in the soil. Although inorganic forms of N (e.g., urea hydrolysis) can also contribute toward the total available N, it is not a significant component in pristine boreal ecosystems and therefore, inorganic N transformations are ignored.

2.3. Feedback Relationships Within BEPS-TerrainLab V2.0

[19] There are number of feedback mechanisms that make a system complex. In BEPS-TerrainLab V2.0, many feedback relationships operate as a result of the tight coupling between hydrological, ecophysiological, and biogeochemical processes. These feedback mechanisms manifest in the form of synergistic or antagonistic effects making many of the processes nonlinear. Some of the important feedback relationships that directly relate to this work are given below.

[20] 1. Increase in plant N increases photosynthesis (term $f(N)$ in equation (A4)) and hence the sizes of biomass and soil C pools due to increased NPP (via equations (1), (2), and (9)). Because of the assumption of first-order kinetics, increased C pool sizes imply increased decomposition and increased N mineralization (term $C_{i,j}$ in equation (C11)) favoring a further increased uptake of plant N (a positive feedback). This feedback mechanism occurs within the model because the N cycle is closely tied to the C cycle.

[21] 2. In humid boreal ecosystems, increase in VSMC beyond the field capacity (term $f(\theta_{sw})$ in equation A34 in the work of *Chen et al.* [2005]) decreases transpiration (term β in equation 2 in the work of *Govind et al.* [2009]) due to plant stress conditions and a consequent stomatal regulation (term $f(\theta_{sw})$ in equation (A1)). Decreased transpiration leads to soil saturation (water balance equation 9 in the work of *Govind et al.* [2009]) resulting in a further decrease of transpiration (a positive feedback). However, soil and moss

evaporations increase as compensatory mechanisms, maintaining the total ET at similar magnitudes.

[22] 3. Decrease in TER at one time step maintains the sizes of C pools (term M in equation (1) and term ΔCx_i in equation (9)). However, this could lead to an increased TER in a future time step (equation (1)) because of the assumption of first-order kinetics (a negative feedback).

[23] 4. Increase in the microbial C pool sizes enhances biological N fixation (term $[C_{sm_i} + C_{m_i}]$ in equation (11)). Consequently, plant N availability increases (equation (10)) facilitating enhanced photosynthesis (term $f(N)$ in equation (A4)) which further increases the sizes of biomass and soil C pools (equations (2)–(3)). This facilitates further microbial proliferation in the soil because of increased substrate availability (equations (B10) and (B11)) (a positive feedback).

[24] 5. Increase in root biomass increase N uptake. This increases photosynthesis (term $f(N)$ in equation (A4)) leading to a further increase in root biomass (equations (2)–(3) and term ΔC_{fr_i} in equation (B4)) which facilitates more N uptake (a positive feedback).

[25] 6. When VSMC falls below the field capacity (term $f(\theta_{sw})$ in equation (A1)), photosynthesis decreases (term g in equations 14a and 14b in the work of *Chen et al.* [1999] and Govind et al. (submitted manuscript, 2009, Figure 7)) because of stomatal regulation. However, decomposition of soil C pools (term M_{s_i} in equation (1); see also Figure 1) and the consequent N mineralization (equation (C11)), could compensate this decrease (a negative feedback). However, if VSMC increases from the permanent wilting point, g_s and N mineralization increases simultaneously favoring a synergistic increase in photosysnthesis as shown by Govind et al. (submitted manuscript, 2009, Figure 7).

[26] 7. Increase in soil water makes the water table depth (WTD) shallower. This increases the root fraction lying in the saturated zone $(1 - \mu)$ (where VSMC = porosity, ϕ) relative to the fraction lying in the unsaturated zone, μ (where VSMC = θ). This effect is proportionately reflected in the physiological status of leaves in the canopy resulting in decreased ET and photosynthesis (equations (A5) and (A6)). This is an indirect positive feedback mechanism that reduces transpiration or GPP because of variations in root wetting patterns as a function of root geometry and local moisture regime.

3. Site Description

[27] The simulation of the coupled biogeochemical and the related feedback mechanisms was conducted on a boreal landscape located southeast of Lake Chibougamau in north central Quebec, Canada (Figure 2). Biogeographically, this region falls under the *Dfc* Köppen climate classification with a mean annual temperature of 0°C and a mean annual precipitation of 961.3 mm (Environment Canada, Canadian Climate Normals or Averages 1971–2000, available at http://www.climate.weatheroffice.ec.gc.ca/climate_normals/index_e.html, accessed 15 May 2007; last update at time of access, 2006). The vegetation consists of an overstory dominated by black spruce (*Picea mariana*) in coniferous stands and aspen (*Populus tremuloides)* or birch (*Betula papyrifera*) in mixed and deciduous stands. Jack pine (*Pinus banksiana*) and tamarack (*Larix laricina*) are sporadically distributed. The understory is mostly dominated by Labrador tea (*Ledum groenlandicum*) and *Salix* sp. The forest floor consists of a thick moss layer; with feather moss (*Pleurozium schrebei*) dominated in wetter areas and *Sphagnum* sp. and lichens in moderately drier areas [*Bergeron et al.*, 2007]. This landscape has a gentle slope of <5%, which is typical of the Canadian Shield. The vegetation species composition varies across the gentle topographic gradient with deciduous and mixed forests in the elevated locations (e.g., eskers) and coniferous species on flatter locations. The soil is derived from glaciofluvial deposits and are mostly podzols having a prominent organic layer with an average depth of 30 cm [*Giasson et al.*, 2006].

4. Flux and Meteorological Measurements

[28] The Eastern Old Black Spruce (EOBS) tower site of Fluxnet-Canada Research Network (FCRN), now the Canadian Carbon Program, is located at 49.69°N and 74.342°W in the southwestern part of this boreal watershed. Eddy covariance (EC) technique is being used at EOBS site to make continuous measurements of CO_2 and energy fluxes since mid-2003. EC instrumentation at EOBS comprises a three-dimensional sonic anemometer, closed and open-path infrared gas analyzers (IRGA) that are mounted on a 24 m scaffold tower. The EC measurements used in this study were quality controlled, gap-filled, and partitioned for flux subcomponents by *Bergeron et al.* [2007] using a standard Fluxnet-Canada algorithm developed by *Barr et al.* [2004]. This algorithm assumes that during night and cold seasons, GPP is negligible and TER equals NEP. Further, daytime TER, missing nighttime and cold season TER were estimated using an empirical logistical function that relates TER and temperature. GEP was further calculated from NEP measurements and TER estimates. These processed data sets were directly obtained from the Data Information System of the Canadian Carbon Program (http://fluxnet.ccrp.ec.gc.ca/) and were used as validation data sets in this study.

[29] Continuous hydrometeorological variables are also being measured at the EOBS tower site. Rainfall is being measured using a tipping bucket rain gauge, and total precipitation is measured using a Geonor T200B rain gauge. WTD is being monitored using piezometers installed at three locations within the EC tower footprint. More details on flux and meteorological measurements can be found in the work of *Bergeron et al.* [2007, 2008]. We used a circular area subtended by a 500 m radius centered on the tower as "the tower footprint" for our data analyses. Since BEPS-TerrainLab V 2.0 runs at daily time steps, we temporally upscaled the meteorological and flux (and flux-derived) measurements taken at half-hourly intervals to a daily time step between January 2004 and December 2005.

5. Spatial Input Data Sets and Initialization of C Pools

[30] Several spatial data sets are required to run BEPS-TerrainLab V2.0. For the present study, we used the same spatial and meteorological data sets used in the hydroecological study of *Govind et al.* [2009]. These spatial data

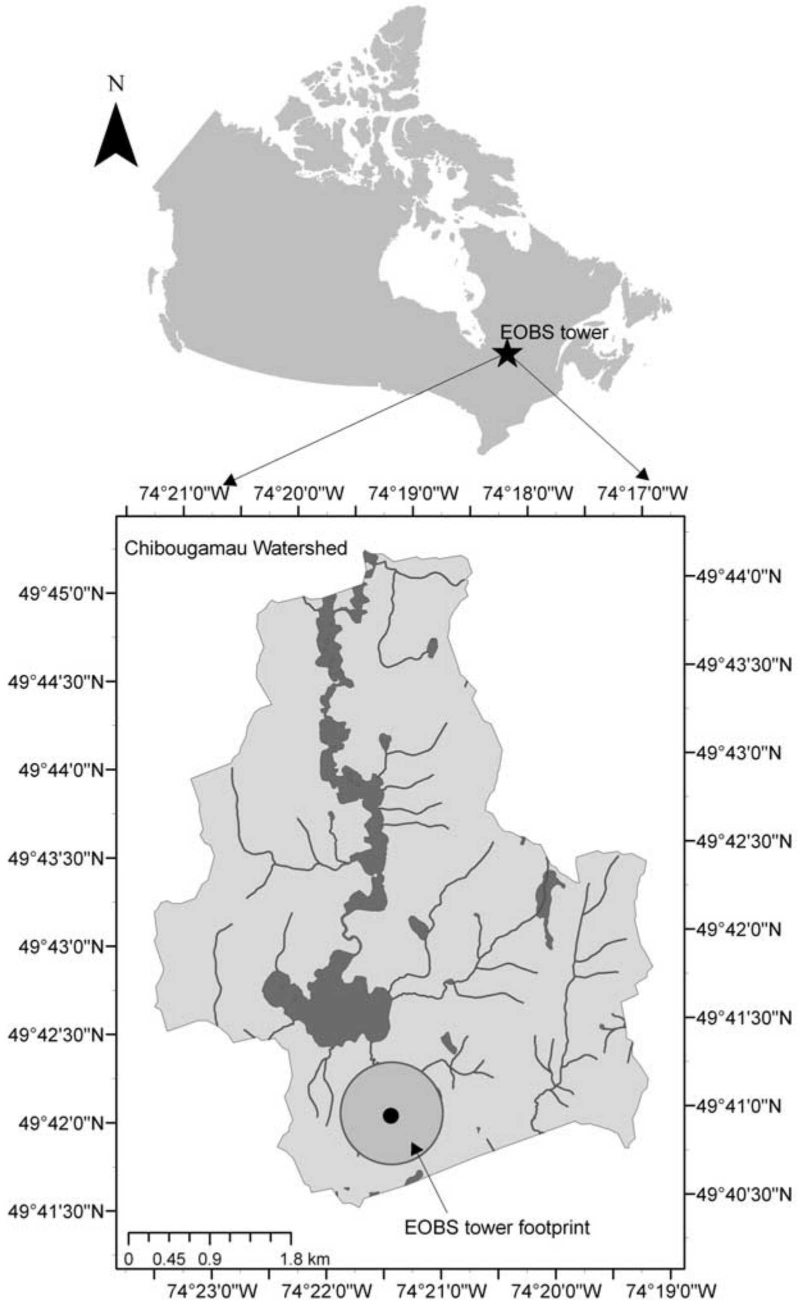

Figure 2. Location of the study site, Chibougamau watershed, which includes the Eastern Old Black Spruce (EOBS) tower site of FCRN where continuous high-precision measurements of fluxes of mass and energy are being made using eddy covariance technique.

sets include maps of (1) land cover, (2) LAI, (3) hydrologically corrected digital elevation model (DEM), (4) slope, (5) aspect, (6) soil texture, (7) initial WTD, (8) spatial distribution of thirteen ecosystem C pool sizes and their C:N ratios for the year 2003 (four biomass C pools and nine soil C pools, i.e., 26 maps), and (9) a DEM-derived watershed boundary. All of these spatial data sets have a common resolution of 25 m and are projected in UTM Z-18N. Daily meteorological variables such as maximum temperature, minimum temperature, dew point temperature, incoming shortwave radiation, wind speed, and precipitation (rain or snow) collected at one point (EOBS tower site) were assigned to all the pixels in the modeling domain after correcting for the effects of elevation and slope on temperature and solar radiation, respectively, using a separate meteorological subroutine within BEPS-TerrainLab V2.0. Biophysical and hydraulic parameters were assigned in a spatially explicit manner on the basis of the land cover and soil maps, respectively. Tables 2a and 2b show some of the important parameters used for modeling ecophysiological and hydrological processes that precede the biogeochemical computations within BEPS-TerrainLab V2.0. Some of the parameters that

Table 2a. Land-Cover-Specific Ecophysiological and Hydraulic Parameters

Ecophysiological Parameters	Units	Conifer	Mixed	Deciduous	Wetlands
Canopy clumping index	-	0.50[a]	0.70[a]	0.80[a]	0.90[b]
Maximum carboxylation rate at 25°C	μmol m^{-2} s^{-1}	33.0[c]	50.0[d]	60.0[d]	33.0[c,e,f]
Maximum stomatal conductance	mm s^{-1}	1.60[a]	3.00[a]	5.00[a]	1.60[f]
Cuticular conductance	mm s^{-1}	0.15[g]	0.15[g]	0.15[g]	0.15[g]
Optimum temperature for photosynthesis	°C	20.0[h,i]	20.0[h]	20.0[h]	20.0[h]
Maximum temperature for photosynthesis	°C	37.0[h]	37.0[h]	37.0[h]	37.0[h]
Root extinction coefficient	-	0.94[j,k]	0.95[j,k]	0.96[j,k]	0.93[j]
Maximum foliar nitrogen	%	1.6[l]	1.7[l]	1.8[l]	1.5[l]

[a] *Liu et al.* [2002] and *Chen et al.* [2006].
[b] *Sonnentag et al.* [2007] and unpublished measurements at a wetland location near the Eastern Old Black Spruce site taken by Ajit Govind, 2006.
[c] *Bonan* [1995] and *Chen et al.* [1999].
[d] After *Wilson et al.* [2001].
[e] Wetlands in the study site have stunted black spruce trees.
[f] *Sonnentag et al.* [2008].
[g] This study.
[h] After *Kimball et al.* [1997] and *Chen et al.* [1999].
[i] *Dang et al.* [1997].
[j] After *Jackson et al.* [1996]. For mixed forests, the value is calibrated between conifers and deciduous.
[k] After *Chen et al.* [2005].
[l] This study.

are exclusively used for biogeochemical modeling are shown in Table 1.

[31] An initialization procedure was employed considering the fact that the quantities and qualities (C:N ratios) of various ecosystem C pools result from the long-term ecological processes subjected to both disturbance and non-disturbance factors. To this end, we used a long-term C cycle model, InTEC [*Chen et al.*, 2000] under climate change, CO_2 fertilization, and N deposition, with the consideration of various disturbance effects on forest age, from 1920 to 2005. This facilitated the spinning-up of all the C pools (biomass and soil C pools) in a spatially explicit manner (Govind et al., manuscript in revision, 2009). We took the values (for all the 13 pool sizes and their C:N ratios) at the end of 2003 as the starting point for intensive biogeochemical simulation using BEPS-TerrainLab V2.0. This initialization procedure is a necessary step because the current sizes of various C pools that act as biogeochemical substrates result from long-term ecological processes. The accuracy of these spun-up C pools was validated using inventory plot measurements taken by the Canadian Forest Service in 2003, in a spatially explicit manner.

6. Modeling Experiments

[32] We hypothesize that lateral subsurface base flow being the most predominant hydrological process responsible for redistributing infiltrated water in humid boreal ecosystems (~65% of annual infiltration), it can significantly affect local-scale hydrological regimes and consequently modulate the ecophysiological and biogeochemical processes. In order to investigate the effects of topographically driven subsurface base flow on the spatial distribution of C sources and sinks (NEP), we conducted a numerical experiment using three modeling scenarios that differ in the manner in which subsurface base flow fluxes are represented. Different scenarios used in this numerical experiment were named "Explicit," "Implicit," and "NoFlow."

[33] In the Explicit scenario, base flow is calculated using explicit topographic controls and has a realistic soil water balance at the local scale (pixel). The Implicit scenario calculates base flow fluxes using a bucket-modeling approach

Table 2b. Land-Cover-Specific Ecophysiological and Hydraulic Parameters[a]

Hydraulic Parameters	Symbol	Unit	Sandy Loam	Peat
Field capacity	θ_{330}	%	0.33[a,b]	0.45[c]
Permanent wilting point	θ_{1500}	%	0.10[b,d]	0.10[c]
Porosity	ϕ	%	0.46[b,e]	0.83[e]
Maximum conductance of soil surface	α	mm s^{-1}	1.0[c]	2.0[c]
Saturated hydraulic conductivity (vertical)	$K_{sat,vertical}$	m d^{-1}	6.0[c]	258[f]
Saturated hydraulic conductivity (horizontal)	$K_{sat,horizontal}$	m d^{-1}	10.0[c]	258[f]
Ks decay rate with depth	σ	m^{-1}	0.03[g]	7.50[f]
Exponent of the moisture release equation	B	–	4.9[b,h]	6.0[i]

[a] *Tombul et al.* [2004].
[b] *Rawls et al.* [1982].
[c] This study.
[d] *Kirchmann et al.* [2005].
[e] *Schwarzel et al.* [2002].
[f] *Govind et al.* [2009].
[g] This study, calibrated.
[h] *Beringer et al.* [2001].
[i] *Letts et al.* [2000].

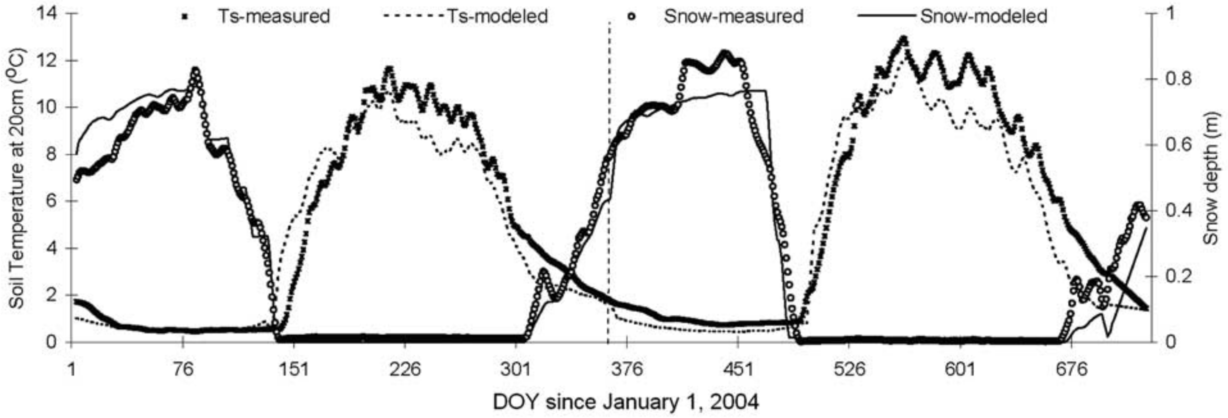

Figure 3. Temporal dynamics of the snow depth and near-surface (20 cm) soil temperature.

assuming that soil water having energy status above the field capacity drains off as lateral flow. In this scenario, neither topographic controls nor interactions of neighboring pixels with regard to lateral water fluxes were considered. This methodology is commonly used in most of the large-scale ecological models where detailed hydrological descriptions are absent (e.g., BEPS [*Liu et al.*, 1997]; CASA [*Potter*, 1997]; and C flux [*Turner et al.*, 2006]).

[34] The third scenario, i.e., the NoFlow, completely ignores the topographically driven subsurface base flow. The only possible pathway of lateral water movement is surface overland flow (SOLF). However, SOLF occurs only after the entire soil profile is saturated. This scheme is employed in models that consider topography-driven lateral water flow but overlooks the consequence of alterations in plant physiological and biogeochemical processes as a result of excessive soil saturation.

[35] In all three scenarios, we used the same spatial data sets, meteorological forcing and land cover and soil-texture-specific coefficients for hydrological, ecological, or biogeochemical processes. In this paper, the Implicit and the NoFlow scenarios are collectively referred to as nonexplicit scenarios. A detailed description of these scenarios and the simulated water balances can be found in the work of Govind et al. (submitted manuscript, 2009).

7. Results

7.1. Snow Depth and Soil Temperature

[36] The simulated dynamics of snowpack thickness and the consequent soil temperature at the EOBS tower footprint is shown in Figure 3 for the years 2004 and 2005. Although we used a quasi-physical approach to model snow dynamics at daily time steps, we were able to capture the seasonal pattern of the snow depth. At the EOBS site, around 25% of the annual precipitation (1053 mm and 902 mm in 2004 and 2005, respectively) was in the form of snowfall, creating an average snowpack thickness of up to 80 cm in March. Much of the discrepancies in the simulated snow depth were seen toward the spring season, especially in 2005, when the model was highly sensitive to air temperature, rain, or solar radiation, which caused a rapid snowmelt. However, in reality, there was a large snowpack built up during this time. Nevertheless, the model captured the dynamics of snow depth on a daily basis (2004–2005) with a reasonable accuracy ($r^2 = 0.90$, $p < 0.001$, and RMSE = 0.07 m d^{-1}).

[37] Snowpack, depending on its density, acts as an efficient thermal insulator that favors edaphic life in the long boreal winter [*Davidson and Janssens*, 2006; *Kielland et al.*, 2006]. Seasonal dynamics of snow depth facilitated realistic simulation of winter soil temperature and various biogeochemical processes. It can be seen from Figure 3 that soil temperature was more or less constant throughout the winter season when the snowpack was present as an insulating layer.

[38] With the inclusion of a multilayer, one-dimensional soil heat transfer procedure, the model was able to capture the annual trend of the near-surface soil temperature (20 cm) with reasonable accuracy ($r^2 = 0.92$, $p < 0.001$, and RMSE = 0.5°C d^{-1}). The inclusion of one dynamic snow layer and five soil layers in order to implement the heat transfer process that is solved numerically utilizing temporally, spatially, and vertically varying thermal properties for a modeling domain that consists of ~50,000 pixels at a daily time step was computationally pragmatic. However, for large modeling domains with finer spatial resolutions, the number of soil layers needs to be reduced or the spatial resolution should be made coarser to implement this scheme.

7.2. Spatiotemporal Patterns of NEP and TER

[39] The spatial distributions of annual NEP for the years 2004 and 2005 are shown in Figure 4. The spatial distributions suggest that, in general, locations that are dominated by mixed and deciduous stands act as C sinks (positive NEP values), whereas mature black spruce stands act as weak C sources, weak C sinks, or as C neutral. There are several studies that demonstrate age-related decline of productivity of mature black spruce stands. Our results are consistent with chrononosequence-based studies conducted in a similar boreal ecosystem by *Wang et al.* [2003] and *Bond-Lamberty et al.* [2004]. Wetlands on this boreal landscape behave as small C sinks, similar to some mature conifer forest stands. The range of the modeled NEP on this boreal landscape was quite large, i.e., −100 to +375 gC m^{-2} a^{-1}, implying a large variability in biogeochemical processes.

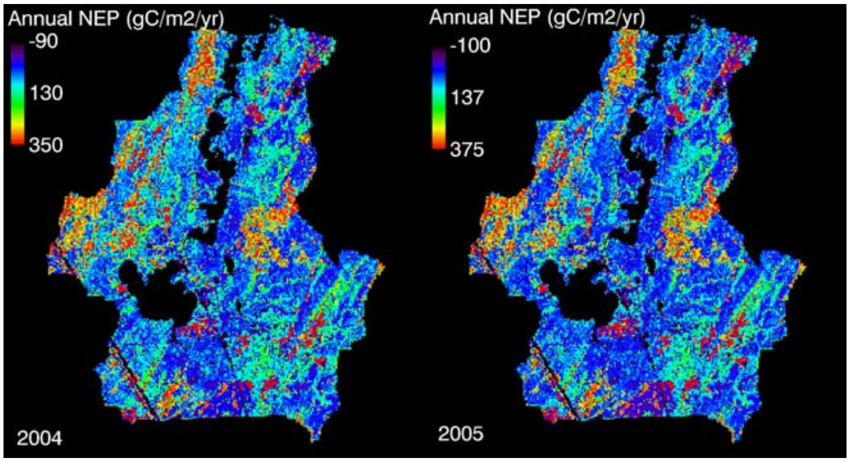

Figure 4. Spatial distribution of the annual net ecosystem productivity (NEP) simulated for the years 2004 and 2005.

[40] We identified that positive annual NEP values were associated with middle-aged stands that are currently acting as large C sinks (~200 gC m^{-2} a^{-1}, locations having red tones in Figure 4). These locations are generally found in deciduous (aspen) or mixed forest-dominated stands that were quickly established after a disturbance event in the recent past. Annual NEP values that we simulated for aspen-dominated stands were consistent with the C fluxes measured in a boreal ecosystem in central Saskatchewan, Canada, by *Krishnan et al.* [2006] who reported an annual NEP of around 153 ± 99 gC m^{-2} a^{-1} in a mature aspen stand. Unlike the spatial distribution of annual GPP [*Govind et al.*, 2009] or NPP (Govind et al., manuscript in revision, 2009), annual NEP showed only a weak congruency with the LAI or land cover distributions.

[41] The simulated temporal patterns of various ecosystem C indicators (GPP, NEP, and TER) in comparison to EC measurements (or EC-derived measurements) taken at the EOBS tower footprint are shown in Figure 5. The temporal pattern of the simulated daily GPP [*Govind et al.*, 2009] is displayed for comparison with NEP and TER. On a daily basis, the model was able to capture the NEP dynamics with reasonable accuracy (r^2 = 0.80, p < 0.001, and RMSE = 0.63 gC m^{-2} d^{-1}). In general, the ecosystem behaved as a C source in the winter and as a C sink in the growing seasons (Figure 5b). In 2004, the annual NEP in the footprint region was simulated to be 11 gC m^{-2} a^{-1} (6 ± 12 gC m^{-2} a^{-1}, measured by EC technique [*Bergeron et al.*, 2007]), and in 2005, it was simulated to be −2.0 gC m^{-2} a^{-1} (0 ± 3 gC m^{-2} a^{-1}, measured by EC technique [*Bergeron et al.*, 2008]). Even during the growing season, on some days, the ecosystem behaved as a strong C source although photosynthesis occurred at higher magnitudes. These conditions usually occurred during warm dry periods (between DOY 150–220 in 2004 and DOY 140–225 in 2005), when TER was much higher than GPP. Similar observations were made by *Griffis et al.* [2003], *Black et al.* [2005], and *Bergeron et al.* [2007] in boreal ecosystems. Meteorological data revealed that 2004 was humid and cooler than 2005, and the flux data showed that in 2004, the annual GPP was around 596 gC m^{-2} a^{-1} while the annual NEP was 6 ± 12 gC m^{-2} a^{-1}. However, in 2005, although the annual GPP was increased to as much as 689 gC m^{-2} a^{-1}, the annual NEP was reduced to 0 ± 3 gC m^{-2} a^{-1}. This implies that although drier and warmer conditions favored increased photosynthesis, it does not necessarily facilitate an increase in C sequestration. We speculate that in this humid boreal ecosystem, warm drier periods favor photosynthesis because of an increase in g_s and N availability. Unlike water-scarce ecosystems where g_s increases or stabilizes even if VSMC increases beyond the field capacity of the soil, in humid boreal ecosystems, a plant stress is induced when VSMC increases beyond the field capacity, which reduces g_s (see Appendix A).

[42] The TER is an influential portion of the C balance determining the NEP of an ecosystem. This is because of the presence of several subcomponent processes (e.g., R_g, R_m and R_h) and the associated feedback mechanisms (e.g., N mineralization) that directly or indirectly modify its magnitude. Components of TER can have different responses to temperature and soil water content [*Boone et al.*, 1998; *Lavigne et al.*, 2004]. Depending on the environmental controls (soil moisture and temperature) and the quantities and qualities of various C pools, the simulated TER implied biogeochemical processes in terms of NEP. In Figure 5c, the simulated TER is compared to the EC-derived TER for the years 2004 and 2005. It can be seen that during the winter seasons, when the air temperature was very low (e.g., −30°C), TER magnitudes were sizable although GPP magnitudes were negligible. During these periods, the near-surface soil temperature remained almost uniform (near 0–1°C) because of the thermal insulation imparted by the snowpack facilitating active soil respiration. Seasonally, 2004 showed smaller shifts in the ecosystem's status as a C sink to C source than 2005, resulting in a net sink of around 11 gC m^{-2} a^{-1}. However, in 2005, although the annual GPP was high, the annual NEP was lower because of increased TER as a result of prolonged warm dry periods. This resulted in simulating the ecosystem as a weak C source (−2 gC m^{-2} a^{-1}). The model was able to capture the seasonal trend of TER with reasonable accuracy (r^2 = 0.84, p < 0.001, and RMSE = 0.54 gC m^{-2} d^{-1}). *Bergeron et al.* [2007] suggests that the thermal insulation created by thick snowpack at the EOBS site makes this

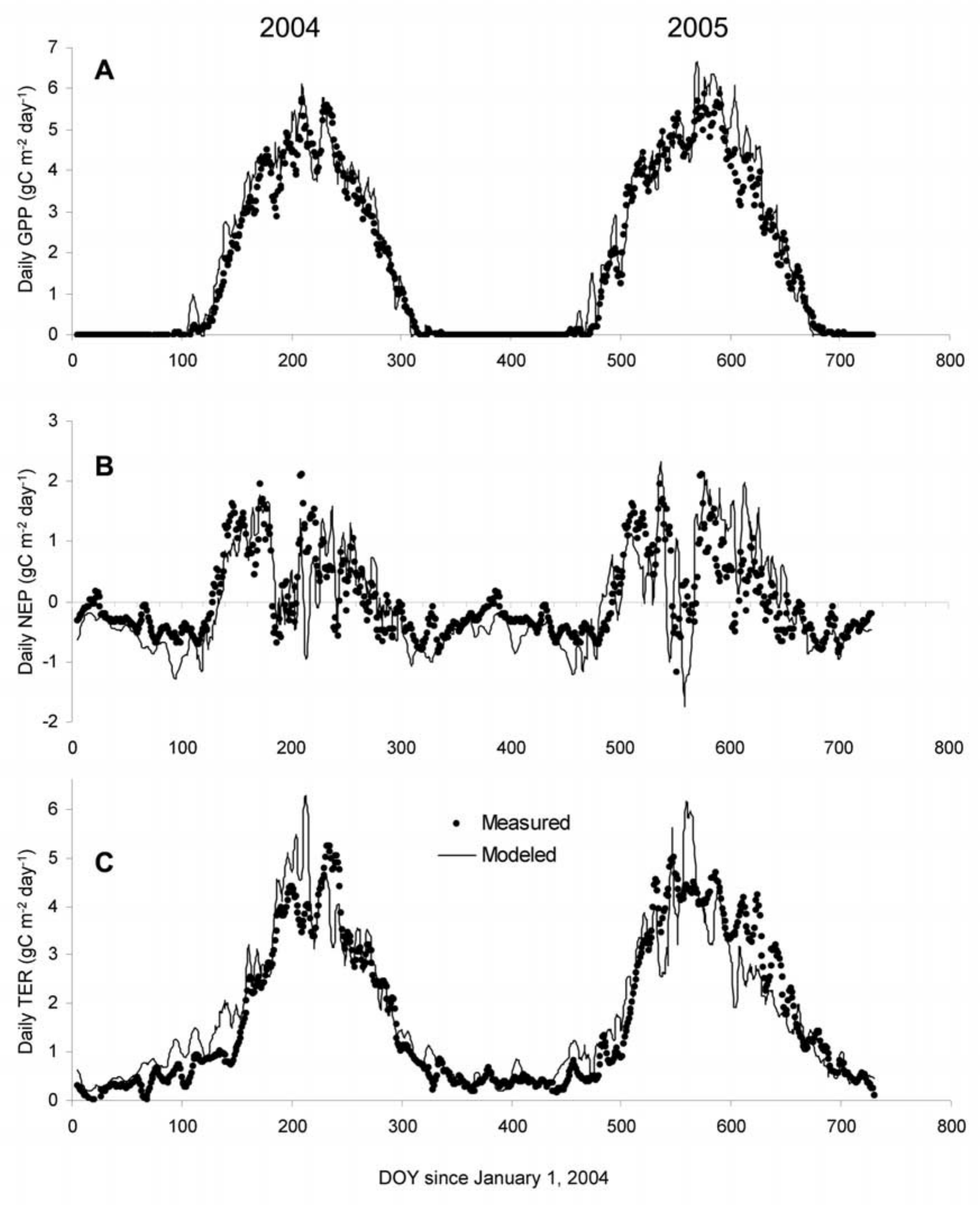

Figure 5. Comparison of measured and simulated (a) gross primary productivity (GPP), (b) net ecosystem productivity (NEP), and (c) total ecosystem respiration (TER) (5-day moving averages shown for visual clarity) at the footprint region of the EOBS tower site for years 2004 and 2005.

ecosystem the smallest C sink in comparison to other mature black spruce ecosystems in Canada.

[43] The increased respiratory losses of C can be attributed to large magnitudes of R_g and R_m, a common characteristic of mature black spruce stands. *Lavigne et al.* [1997] reported that for black spruce ecosystems, soil respiration accounts for as much as 48–71% of TER. *Black et al.* [2005] also reported that the contribution from soil respiration can be as high as 80, 67, and 83% of TER for boreal aspen, black spruce, and jack pine sites, respectively. We recognize that the presence of thick snowpack in the winter season has a great role in determining the annual NEP of C neutral ecosystems. *Goulden and Crill* [1997], *Goulden et al.* [1998], and *Black et al.* [2005] also suggest that boreal coniferous stands can release a large amount of the C gained in the previous growing season because of respiratory losses during winter. Thus, modeling snow dynamics is critical to

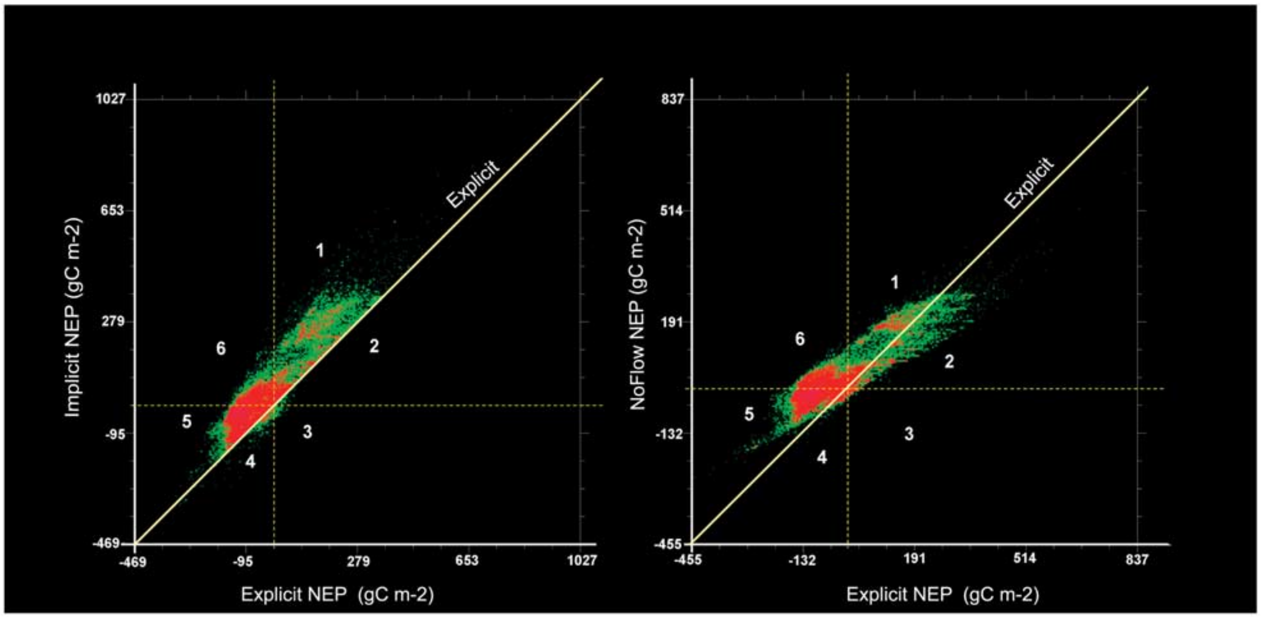

Figure 6. Plots of the annual NEP simulated under different hydrological scenarios. (left) The plot between the Implicit and Explicit scenarios. (right) The plot between the NoFlow and the Explicit scenarios. In both plots, the line on slope = 1 is the Explicit scenario, and departure from this line is considered as the bias.

accurately simulate soil temperature, soil respiration, and thus NEP in mature boreal ecosystems.

[44] We also need to consider some feedback mechanisms that are strengthened because of temporal variations in TER, GPP, and ET to fully understand the C balance of this humid boreal ecosystem. For example, while R_a is primarily determined by the magnitudes of various biomass C pools and temperature, R_h is determined by a variety of factors such as soil temperature, soil moisture, quantities and qualities of various soil C pools and some feedback relationships. During warm dry periods, increased ET losses rapidly dried the soil profile which facilitated increased decomposition of soil C pools that resulted in increased N mineralization and leaf N. This affected GPP due to increased carboxylation rates. Thus, we speculate that the increased NEP (sink) immediately after prolonged dry periods could be partially attributed to photosynthetic gains due to the synergism between increased N mineralization and increased g_s due to optimal soil moisture conditions (between permanent wilting point and field capacity).

7.3. Differences in the Simulated Annual NEP Under Hydrological Scenarios

[45] In order to investigate the role of hydrological processes that govern the local-scale biogeochemical processes and the consequent spatial distribution of C sources and sinks, we analyzed the annual NEP (2004) simulated by the three hydrological scenarios as described in section 6. Before analyzing the differences in simulated biogeochemical processes, it is useful to understand how hydrological processes differ under the three scenarios. Govind et al. (submitted manuscript, 2009) describes the variations in the water balance at the footprint region of the EOBS tower site for all the three scenarios. It was suggested that 93% of the annual precipitation entered the soil as infiltrated water after accounting for canopy interception and evaporation. Of this infiltrated water, 64.4%, 76.2%, and 0% were lost as subsurface base flow; 7.9%, 0%, and 66% were lost as SOLF; 27%, 32.4%, and 24.5% were lost as ET (excluding evaporation of water intercepted on the canopy); and +0.05%, −8.6%, and +9.4% were the storage changes in the Explicit, Implicit, and the NoFlow scenarios, respectively. It is hence clear that subsurface base flow is the dominant mechanism of water partitioning in the Explicit and the Implicit scenarios whereas it is SOLF in the NoFlow scenario. Nevertheless, the magnitudes of total lateral water fluxes (base flow +SOLF) is similar in all the three scenarios i.e., 72%, 76%, and 66% of the annual infiltrated water in the Explicit, Implicit, and the NoFlow scenarios, respectively, indicating that it is the nature of hydrological partitioning that creates differences in the biogeochemical simulations.

[46] Figure 6 shows a pixel-to-pixel comparison of annual NEP simulated under the three scenarios (Explicit versus Implicit or NoFlow scenarios) for the whole watershed (n = 35426). The color tones represent the density of annual NEP values. Red tones indicate the most commonly occurring values whereas green tones indicate annual NEP values that are rarely found on this boreal landscape. The plots clearly demonstrate that there are pronounced differences under the three hydrological scenarios (deviation from the 1:1 line).

[47] In general, both the nonexplicit scenarios overestimated annual NEP in comparison to the Explicit scenario. Since NEP depends on many processes such as photosynthesis, TER, N mineralization, g_s, and the associated feedback relationships that are intensified by hydrothermal variations directly or indirectly, it is impossible to give a single reason for the differences in the simulated annual NEP. It is probable that TER is greatly subdued under the NoFlow scenario resulting in an increased annual NEP (as

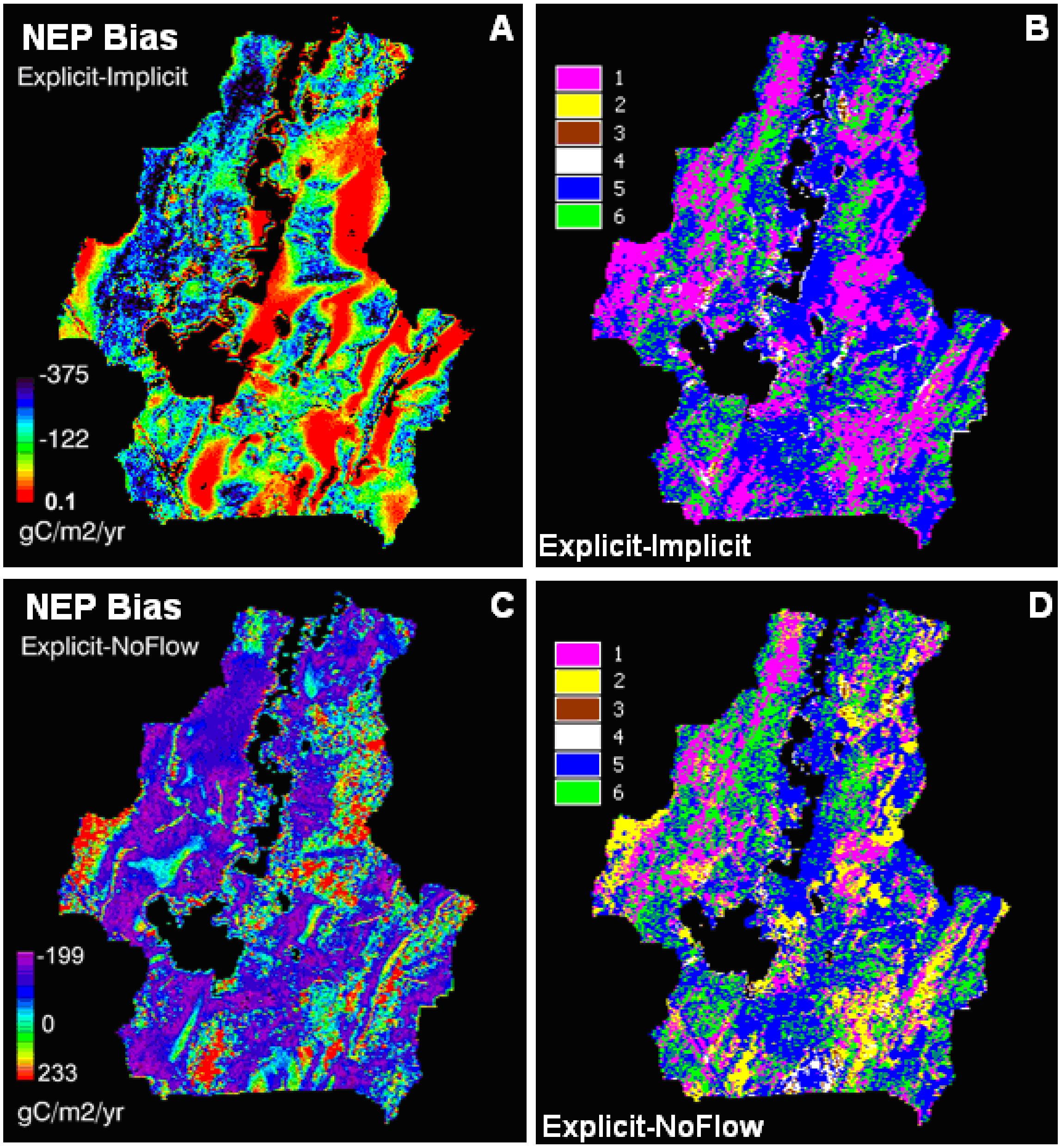

Figure 7. The spatial distribution of annual NEP bias under various hydrological scenarios: (a) by the Implicit scenario and (c) by the NoFlow scenario. (b and d) The spatial distribution of NEP difference types for the Implicit and the NoFlow scenarios, respectively.

much as 199 gC m^{-2} a^{-1}). This could be because of excessive soil saturation that makes the ecosystem a net C sink in spite of having lowered photosynthesis due to decreased g_s (due to flooding-induced plant stress) and decreased N mineralization (due to reduced decomposition of soil C pools). The deviation created by the NoFlow scenario resembles the type of bias inherently present in models where the lateral water fluxes are assumed to be only due to SOLF. This is a common type of hydrological representation in some of the land surface schemes that are used within GCMs [*Shao and Henderson-Sellers*, 1996].

[48] The Implicit scenario also showed, in general, an overestimation of the annual NEP in comparison to the Explicit scenario. This could be due to optimal soil moisture conditions that favored photosynthetic C gains (due to an increase in g_s and N availability) that dominated over increased respiratory C losses. Implicit calculation of subsurface base flow assumed that within a soil profile, if soil water has energy status above the field capacity, it is prone to gravitational flow. However, base flow in this scenario is not directly controlled by topography. Thus, even on flatter locations, where the slope is almost negligible, soil moisture conditions unrealistically remained conducive for plant growth and decomposition of soil C pools. Implicit formulations of lateral water fluxes are common in ecological models such as *Liu et al.* [1997], *Turner et al.* [2006], or *Potter* [1997] where hydrological controls are implicitly

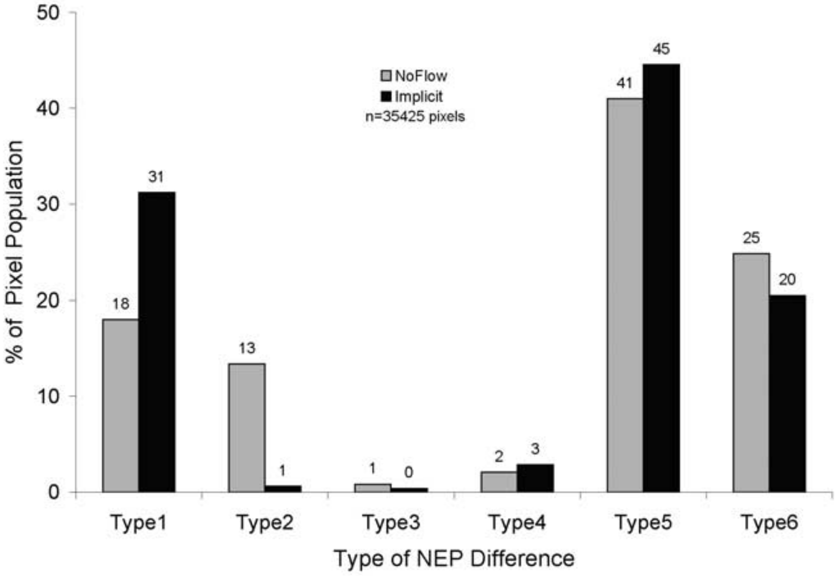

Figure 8. Relative occurrence of various NEP difference types under different hydrological scenarios. Note that in both the nonexplicit scenarios, type 5 is the dominant bias type.

represented irrespective of the topographic variations of the landscape.

[49] Figures 7a and 7c show the spatial distributions of the differences of the annual NEP as simulated by the nonexplicit scenarios in comparison to the Explicit scenario (hereafter "NEP difference"). It is quite apparent that NEP differences were prominent in both of the two nonexplicit scenarios. The spatial distribution of NEP differences between the Implicit and the Explicit scenarios (Explicit-Implicit) shows that there is a marked overestimation of the annual NEP by the Implicit scenario (dark blue tone, -ve values represent overestimation). On flatter soil-saturation-prone locations, annual NEP was greatly overestimated (as much as 375 gC m^{-2} a^{-1}). At these locations, if the land cover was composed of deciduous or mixed forests, photosynthesis and N availability synergistically increased, which further overestimated the annual NEP. On hillslope locations, the Implicit scenario created only slight underestimations (red tone) because the simulated base flow fluxes were comparatively lesser than what the Explicit scenario would simulate. Note that the maximum underestimation by the Implicit scenario on hillslopes was as low as 0.1 gC m^{-2} a^{-1}, indicating that the Implicit scenario has only a weak tendency to underestimate NEP.

[50] The spatial distribution of NEP differences between the NoFlow and the Explicit scenarios (Explicit−NoFlow) also show that there is, in general, an NEP overestimation (blue tone, low values represent overestimation). On flatter locations, annual NEPs were overestimated (as much as 199 gC m^{-2} a^{-1}) whereas on some locations, unlike the Implicit scenario, the NoFlow scenario showed marked underestimation of annual NEP probably because of an antagonistic reduction of photosynthesis due to reduction in g_s and N mineralization.

[51] Interpreting the influence of topographically driven base flow on biogeochemical processes solely on the basis of NEP difference maps is inadequate because various factors affect these processes simultaneously and differently. In the scatterplots shown in Figure 6, it is possible to delineate NEP differences into six types. Each NEP difference type has a unique reason for its occurrence. These can be summarized as follows:

[52] Type 1: This type of bias occurs when the NEP simulated by the nonexplicit scenario is larger than the Explicit scenario. This is a case of intensification of an existing C sink, and this bias arises either from an increase in GPP and/or a reduction in TER.

[53] Type 2: This type of bias occurs when the NEP simulated by the nonexplicit scenario is less than the Explicit scenario. This is a case of weakening of C sinks, and this bias arises either from a decrease in GPP and/or an increase in TER.

[54] Type 3: This type of bias occurs when the NEP simulated by the nonexplicit scenario results in a complete reversal of C sinks (mostly weak sinks) to C sources.

[55] Type 4: This type of bias occurs when the NEP simulated by the nonexplicit scenario intensifies the existing C sources because of an increase in TER and/or a reduction in GPP.

[56] Type 5: This type of bias occurs when the NEP simulated by the nonexplicit scenario weaken the C sources but still remain as C sources because of a small decrease in TER and/or a small increase in GPP.

[57] Type 6: This type of bias occurs when the NEP simulated by the nonexplicit scenario results in a complete reversal of C sources (mostly weak sources) to C sinks because of an increase in GPP and/or decrease in TER.

[58] In order to get a better insight on the effects of subsurface base flow on biogeochemical processes, we mapped the NEP difference types as shown in Figures 7b and 7d for the two nonexplicit scenarios. It is obvious that type 5 and type 1 are the dominant forms under the Implicit scenario and type 5, type 1, and type 2 in the NoFlow scenario. Hence, it can be deduced that errors in the simulated NEP as a result of simplified hydrological representations can have various reasons for their existence.

Table 3. Differences in the Magnitudes of C Fluxes Within Various NEP Difference Types as a Result of Nonexplicit Hydrological Representation

Bias Type	ΔNEP[a] (as %)	ΔGPP[a] (as %)	ΔRa[a] (as %)	ΔRh[a] (as %)	Dominant Mechanism	Probability of Occurrence[b]
				Implicit		
1	+60.1	+16.3	+8.3	+8.7	P dominated sink increase	31.2
2	−5.1	+31.3	+37.9	+37.3	R dominated sink decrease	0.6
3	−245.1	+119.5	+128.7	+131.9	R dominated sink to source	0.4
4	−17.4	+57.5	+52.7	+52.1	R dominated source increase	2.9
5[c]	+52.4	+15.0	+7.3	+5.1	P dominated source decrease	44.5
6	+166.0	+25.9	+12.3	+9.6	P dominated source to sink	20.5
				NoFlow		
1	+43.8	−21.7	−29.7	−31.7	P dominated sink increase	18.0
2	−24.2	−32.3	−33.2	−35.5	R dominated sink decrease	13.4
3	−172.5	−30.5	−24.5	−28.9	R dominated sink to source	0.8
4	−42.1	−18.9	−13.1	−18.0	R dominated source increase	2.1
5[c]	+68.6	−35.9	−39.9	−40.7	R dominated source decrease	41.0
6	+138.0	−29.6	−38.2	−39.8	P dominated source to sink	24.8

[a] Percentage change from Explicit values of annual net ecosystem productivity (NEP), gross primary productivity (GPP), Ra, and Rh. *P* is photosynthesis, and *R* is respiration.

[b] As percentage of n = 35425 pixels.

[c] Dominant bias type.

Figure 8 shows the relative contribution of different types of biases under the nonexplicit scenarios. It is clear that type 5, type 1, and type 6 are the dominant types of NEP biases.

8. Discussion

8.1. Mechanisms of Hydrological Control on NEP

[59] In section 7.3, it was demonstrated that alterations in local hydrological regimes as a result of differences in the conceptualization of the landscape-scale hydrological processes can greatly affect the spatial distribution of annual NEP. These NEP differences occur mainly because of variations in the magnitudes of the two hydrologically controlled processes, GPP and TER. Table 3 summarizes the mechanisms of NEP differences under the three scenarios. In Table 3, ΔNEP, ΔGPP, ΔRa, and ΔRh represent percentage change in NEP, GPP, Ra, and Rh as a result of nonexplicit hydrological representation relative to the Explicit scenario (realistic). Because of nonlinearities and feedback relationships, these changes are not additive in nature. It can be seen that a type 5 bias is mainly responsible for overestimation of annual NEP in both the nonexplicit scenarios. Under the Implicit scenario, the type 5 bias is responsible for errors in 44.5% of the pixel population. Under the NoFlow scenario also, a type 5 bias is still the dominant cause for NEP errors (errors in 41% of the pixel population). Although a type 5 bias is created because of weakening of C sources, it should be noted that the mechanisms are quite different in both nonexplicit scenarios.

[60] In the Implicit scenario, a type 5 bias occurs mainly because of a 15% increase in GPP. Here, the soil moisture status is always maintained at optimal conditions (between field capacity and permanent wilting point) which increases g_s at locations that are otherwise saturated (e.g., flat and lowlands). Increased g_s leads to increased transpiration and photosynthesis. Consequently, conducive conditions for soil respiration and decomposition of soil C pools are created leading to N mineralization [*Arain et al.*, 2006; *Traore et al.*, 2007; *Tan and Chang*, 2007] which synergistically increases GPP on the basis of the feedback mechanisms 1, 4, and 5 as shown in section 2.3. There are physiological studies that demonstrate that optimal moisture conditions increase available plant N which further affects Vcmax and photosynthesis positively [*Wohlfarht et al.*, 1999]. The temporally integrated Farquhar model of *Chen et al.* [1999], which is employed in BEPS-TerrainLab V2.0, has a nonlinear relationship between g_s and photosynthesis (Govind et al., submitted manuscript, 2009). However, because of the synergism between N availability and g_s, GPP steadily increases under the Implicit scenario without any saturation. This causes a positive bias in the simulated NEP even if the TER is enhanced simultaneously.

[61] Under the NoFlow scenario, a type 5 bias occurs mainly because of suppression of TER (40%), even if the photosynthesis reduces as much as 35%. Feedback mechanisms (2, 3, 6, and 7 mentioned in section 2.3) that operate under the NoFlow scenario facilitate unrealistic reduction of photosynthesis because of reduction in g_s and N availability due to soil saturation. However, the respiratory losses are greatly suppressed under this scenario creating a net gain in NEP.

[62] In general, the net effect in both the nonexplicit scenarios is a weakening of the existing C sources (NEP becoming less negative). This reveals that ecological models that have simplified hydrological representations could have larger errors in determining the magnitudes of existing C sources rather than the C sinks. Although the lateral water fluxes (as the sum of subsurface base flow and SOLF) simulated by all the three scenarios are comparable, these simplified hydrological representations introduce unrealistic plant physiological and biogeochemical conditions creating systematic errors that intensify many feedback mechanisms within modeling domains.

8.2. Dynamics of Ecosystem C Pools Under Various Hydrological Scenarios

[63] Although it is obvious that the magnitudes of annual GPP and annual TER determine annual NEP, it is also important to understand the nature of C dynamics (both in the biomass and in the soil) under the three hydrological

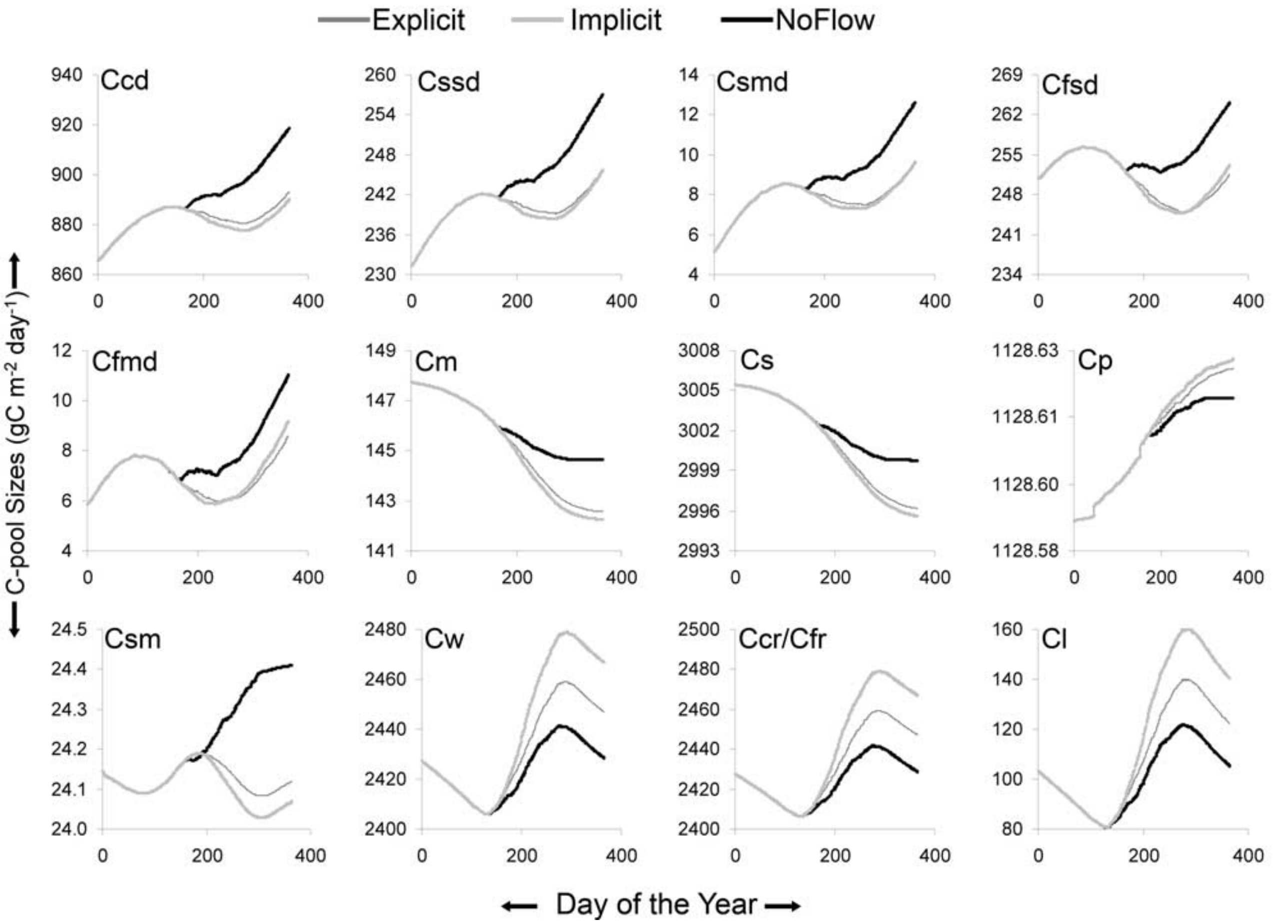

Figure 9. Temporal dynamics of various ecosystem C pools under hydrological scenarios. The C pools shown here are coarse detritus pool (C_{cd}), surface structural pool (C_{ssd}), surface metabolic pool (C_{smd}), soil structural litter pool (C_{fsd}), soil metabolic pool (C_{fmd}), soil microbial pool (C_m), slow C pool (C_s), passive C pool (C_p), surface microbial pool (C_{sm}), woody biomass pool (C_w), coarse root and fine root biomass pools combined (C_{cr} C_{fr}), and foliage biomass pool (C_l).

scenarios. Ecosystem C pools act as substrates for various biogeochemical processes. Sizes of C pools are important in determining the magnitudes of the subcomponents of TER or N mineralization because a first-order kinetics is assumed to describe these biogeochemical processes in most of the ecological models similar to BEPS-TerrainLab V2.0. Moreover, these trends are likely to shed some light on the current uncertainties associated with the terrestrial C cycle under climate change [e.g., *Cox et al.*, 2000]. The temporal dynamics of various biomass and soil C pools (landscape average) for the three scenarios are shown in Figure 9 for the year 2004. It is apparent that the differences among the scenarios are identifiable soon after the spring (~DOY = 150) when soil gets wet because of snowmelt, initiating base flow fluxes.

[64] The soil C pools, C_{cd}, C_{ssd}, C_{smd}, C_{fmd}, C_{fsd}, C_m, C_s, and and C_m accumulate under the NoFlow scenario and tend to deplete under the Implicit scenario. This is because soil moisture in the former case was suboptimal for C pool decomposition while it was hyperoptimal in the latter case. Only the passive soil organic C pool (C_p) showed a trend different from the other soil C pools. This is theoretically plausible because C_p represents the most recalcitrant form of soil C that comprises humus, which is the last product of soil organic matter decomposition. Because C decomposition was intense in the Implicit scenario, C_p accumulated as opposed to the NoFlow scenario. On the other hand, biomass C pools (C_w, C_{cr}, C_{fr} and C_l) were underestimated in the NoFlow scenario while they were overestimated the Implicit scenario. This is mediated by changes in g_s, variations in R_a, and N mineralization.

[65] Figure 10 demonstrates how the soil C stocks (sum of all soil C pools) build up in the soil under the NoFlow scenario. Under saturated conditions, the model simulated the C cycle similar to temperate wetlands where the decomposition of soil organic matter is very limited [*Nakane et al.*, 1997; *Bond-Lamberty et al.*, 2007]. However, under the Implicit scenario, the soil C pools decomposed faster in the growing season, although sufficient replenishments occurred because of increased biomass C turnover into the soil.

8.3. Nutrient (N) Availability and Associated Feedback Mechanisms

[66] N control on C cycle is represented in BEPS-TerrainLab V2.0 through leaf N that affects the Vcmax used in the process-based photosynthesis model [*Arain et*

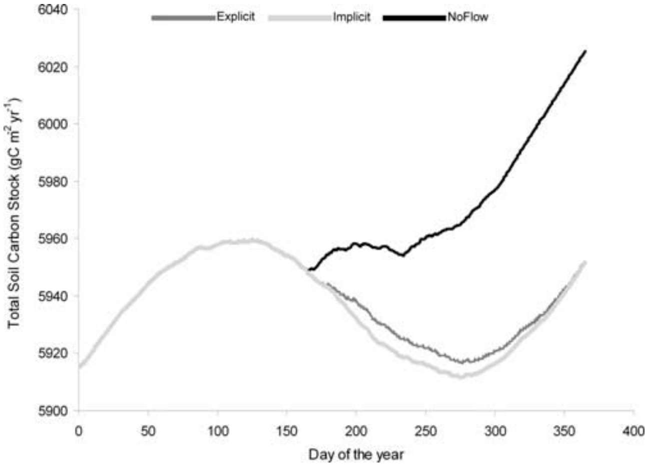

Figure 10. Temporal dynamics the total soil C pools (sum of all the pools) under various hydrological scenarios.

al., 2006]. Although a substantial amount of N is present in the soil organic matter, a majority of this is unavailable to plants. Since BEPS-TerrainLab V2.0 simulates the sizes of various soil C pools, it is possible to simulate the dynamics of their C:N ratios as well (see Appendix B for the equations). The dynamic nature of the quantities and qualities of C pools facilitates the calculation of N mineralization or immobilization that occurs as a result of soil C pool decomposition or interconversion. Together with N_{dep} and N_{fix}, only part of the soil N is available to the vegetation. This continuum of N cycling in the soil is strongly controlled by hydrothermal processes. The Implicit scenario mimics conditions that are seen in well-drained deciduous forests while the NoFlow scenario mimics conditions similar to peatlands [*Devito et al.*, 1999].

[67] Figure 11 shows the seasonal pattern of leaf N (%) under the three hydrological scenarios. Leaf N remained minimal in the winter seasons, owing to weak decomposition of soil C pools and N availability, under all the scenarios. In the NoFlow scenario, in general, the soil water balance was altered in such a way that soil profile got excessively saturated because of the absence of topographically driven base flow. Under the NoFlow scenario, although the possibility of some locations becoming excessively dry cannot be fully ruled out, because of the excessively humid nature of this ecosystem, it can be generalized that locations that dry because of the absence of base flow fluxes are comparatively less. Throughout the year, soil C pools accumulate without decomposition, reducing N mineralization. However, under the Implicit scenario, soil moisture remains conducive even on flatter locations of the landscape creating optimal conditions for N mineralization and biomass increase. This increased biomass further increases C inputs to soil thus facilitating more N mineralization, creating a positive feedback mechanism [*Schroter et al.*, 2003].

9. Summary and Conclusions

[68] In order to better understand the interactions between water, C, and N cycles in terrestrial ecosystems in a spatially explicit manner, we developed a hydroecological model, BEPS-TerrainLab V2.0 that has a tighter coupling of ecophysiological, hydrological, and biogeochemical processes. We ran this model over a boreal landscape in north central Quebec and compared the simulations with various measurements to test the model's performance. Further, we conducted a modeling experiment to understand the hydrological influence on C and N cycling and the associated feedback mechanisms. From this study we draw the following conclusions.

[69] 1. The seasonal dynamics of modeled NEP and TER at a daily time step agreed well with the eddy covariance measurements indicating that BEPS-TerrainLab V2.0 can capture these biogeochemical processes with reasonable accuracy.

[70] 2. The main factors governing the accuracy of the simulated NEP were the accuracies of the simulated GPP and TER. While the former depends mainly on hydrologically controlled g_s and the leaf N content, the latter depends on several factors that directly or indirectly depend on soil hydrothermal regimes and the nature of the dynamics of various ecosystem C pools.

[71] 3. Accuracies of TER (particularly R_h) and N mineralization are thermally controlled. It is therefore essential to precisely model boreal edaphic thermal regimes in order to accurately map C sources and sinks. This needs the inclusion of snow dynamics and soil heat transfer schemes within ecological models that simulate C dynamics in boreal ecosystems.

[72] 4. In general, hydrological simulations without the explicit consideration of subsurface base flow overestimate NEP. Six types of biases can be created because of simplified hydrological representations. These biases occur because of variations in ecophysiological and biogeochemical processes consequent of the nature of the local-scale soil water balance. The most common bias is an underestimation of the existing C sources.

[73] 5. Soil C dynamics are significantly altered under simplified hydrological representations. Soil C pools either accumulate as the soil saturates due to decrease in TER or deplete when soil moisture is maintained at hyperoptimal conditions. This has significance with regard to N avail-

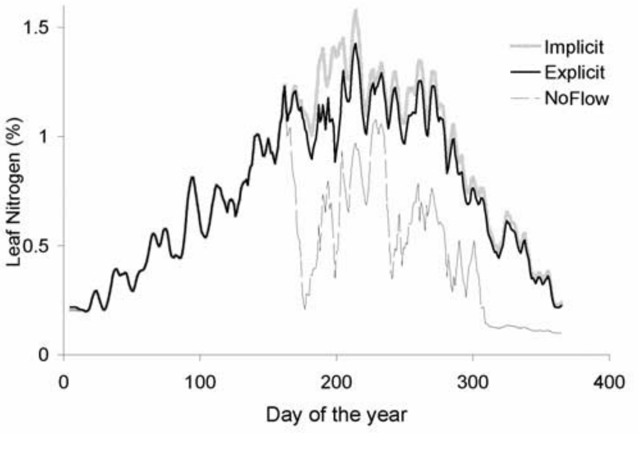

Figure 11. Temporal dynamics of leaf N content under various hydrological scenarios. Note the pronounced N limitation under the NoFlow scenario which is primarily due to reduced soil C decomposition and N mineralization.

ability, which indirectly affects primary production and C cycling.

[74] In conclusion, we saw that hydrology plays a critical role in determining the spatiotemporal distribution of C sources and sinks. We believe that it is imperative to simulate realistic hydrological regimes within ecological models to accurately map spatiotemporal patterns of C sources or sinks. Our results suggest that the lateral subsurface flow does play a significant role in boreal C source/sink distribution. Some studies indicate that under climate change, melting of permafrost in high-latitude ecosystems could intensify biogeochemical processes [*Deming*, 1995; *Zimov et al.*, 2006]. Large-scale bottom-up modeling endeavors should therefore have a tight coupling of hydrological, ecophysiological, and biogeochemical processes to reduce the current uncertainties in terrestrial-atmosphere C exchange.

Appendix A

A1. Ecophysiological Processes

A1.1. Ambient Stomatal Conductance (g_s)

[75] In BEPS-TerrainLab V2.0, g_s is calculated similar to the multiplicative approach proposed by *Jarvis* [1976]. Scalars (ranging between 0 and 1) representing various environmental controls constrain a land-cover-specific maximum stomatal conductance, $g_{s,\max}$ to return the g_s as shown below:

$$g_\mathrm{s} = g_{s_\mathrm{max}} \cdot \left[f\left(F_\mathrm{p}\right) \times f(T_a) \times f(D_\mathrm{v}) \times f(\theta_\mathrm{sw}) \times f(T_s) \right] \tag{A1}$$

Here F_p is the photosynthetic photon flux density (PPFD), T_a is the mean air temperature, D_v is vapor pressure deficit, and θ_{sw} is the VSMC. There are many studies that provide evidence that either g_s or ET decreases with increasing θ_{sw} beyond the field capacity [*Pereira and Kozlowski*, 1977; *Kozlowski*, 1984; *Zhang and Davies*, 1987; *Else et al.*, 1996]. Flooding-induced plant stress occurs because of a variety of reasons such as anoxic conditions and production of toxic compounds in the rhizosphere. Unlike water-limited ecosystems, where plant stress is a direct function of water scarcity, in humid boreal ecosystems, water stress is mostly attributed to soil saturation (flooding). In order to conceptualize this, in BEPS-TerrainLab V2.0 we use $f(\theta_\mathrm{sw})$ which is unique to boreal ecosystems. The method for calculating these scalars can be found in the works of *Chen et al.* [2005, 2007] and *Sonnentag et al.* [2008]. In BEPS-TerrainLab V2.0 a new scalar $f(T_s)$ accounts for the effects of soil temperature on g_s [*Govind et al.*, 2009]. Finally, the total conductance is calculated by assuming the cuticular conductance $g_{cuticle}$ in parallel and boundary layer conductance $g_{boundary}$ in series to g_s. Conductance for CO_2 transport between the vegetation and the atmosphere is assumed to be 0.0625 times the conductance for H_2O.

A1.2. Photosynthesis

[76] Daily canopy-scale photosynthesis is calculated using the instantaneous leaf-level model of *Farquhar et al.* [1980], which is approximated as the minimum of Rubisco-limited and light-limited gross photosynthesis rates as shown below:

$$A = \min\left(W_c, W_j\right) - R_d \tag{A2}$$

$$W_c = V_m \frac{C_i - \Gamma}{C_i + K} \text{ and } W_j = J \frac{C_i - \Gamma}{4.5C_i + 10.5\Gamma} \tag{A3}$$

where A is the net leaf-level photosynthesis and W_c and W_j are Rubisco-limited and light-limited gross photosynthesis rates in mmol m^{-2} s^{-1}, respectively. R_d is the dark respiration. V_m is the maximum carboxylation rate while J is electron transport rate. C_i is the intercellular CO_2 concentration; K is a function of enzyme kinetics. Γ is the CO_2 compensation point without the effects of dark respiration. V_m can be expressed as a function of both temperature and leaf nitrogen content [*Bonan*, 1995]:

$$V_m = V_{m25} . 2.4^{\frac{(T-25)}{10}} . f(T) . f(N) \tag{A4}$$

[77] For daily applications, *Chen et al.* [1999] developed a temporal upscaling scheme by equating equation (A2) with $g(C_i - C)$, another representation for leaf-level photosynthesis [*Leuning*, 1990]. Furthermore, this temporally upscaled model is spatially upscaled using LAI fractions that correspond to different physiological statuses (four-leaf approach) for the overstory canopy (equation (A5)) and big-leaf approach for the understory and the moss layers:

$$\begin{aligned} A_{canopy} = {} & \left[A_{sun,unsat} LAI_{sun} \cdot \mu + A_{sun,sat} LAI_{sun}(1-\mu)\right] \\ & + \left[A_{shade,unsat} LAI_{shade} \cdot \mu + A_{shade,sat} . LAI_{shade}(1-\mu)\right] \end{aligned} \tag{A5}$$

[78] In equation (A5), A_{ij} is the daily leaf-level photosynthesis calculated separately for four physiologically distinct leaf types in a canopy. These physiological variations are conceptualized on the basis of differences in light, i (sunlit or shaded) and water regimes, j (saturated or unsaturated), creating unique values of g_s. Here, j is calculated on the basis of the assumption that the nature of root-wetting pattern proportionately reflects in the physiological statuses of leafs in a canopy through the variable, μ which is a function of the root extinction coefficient, β (Table 2) and WTD. Root fraction $(1 - \mu)$ lying in the saturated zone gets VSMC = θ_s = ϕ whereas root fraction (μ) lying in the unsaturated zone gets VSMC = θ [*Govind et al.*, 2009].

$$\begin{aligned} A_{sun,sat} &= f\left(g_{s,sun,sat}\right) & g_{s,sun,sat} &= f_1\left(F_{p_{sun}}, \phi\right) \\ A_{sun,unsat} &= f\left(g_{s,sun,sat}\right) & g_{s,sun,sat} &= f_1\left(F_{p_{shade}}, \theta\right) \\ A_{shade,sat} &= f\left(g_{s,shade,sat}\right) & g_{s,sun,sat} &= f_1\left(F_{p_{sun}}, \phi\right) \\ A_{shade,unsat} &= f\left(g_{s,shade,unsat}\right) & g_{s,sun,sat} &= f_1\left(F_{p_{shade}}, \theta\right) \end{aligned} \tag{A6}$$

LAI = Total leaf area index from the input data.

$$LAI_{sun} = 2.\mathrm{Cos}\theta . \left(1 - \exp\left[-\frac{0.5.\Omega.LAI}{\mathrm{Cos}\theta}\right]\right) \tag{A7}$$

LAI_{sun} is the sunlit LAI, θ = solar zenith angle, and Ω is canopy clumping index (Table 2).

$$LAI_{shade} = LAI - LAI_{sun} \tag{A8}$$

LAI_{shade} is the shaded LAI.

[79] Leaf-level photosysnthesis, $A_{i,j}$ for each radiation (i) and hydrologic regime (j) within a canopy is calculated on the basis of the function, f, which is equation (A2) using unique stomatal conductance values based on the function, f_1 (Jarvis algorithm) as shown in equation (A6).

Appendix B: Dynamics of Various Ecosystem Carbon Pools

CN_x	C:N ratio of a C pool, x; e.g., CN_{cr} is the C:N ratio of coarse root biomass pool.
C_x	C content in pool x in gC m^{-2}; e.g., C_{cr} is the C content in the coarse root biomass pool.
i	Day of the simulation.
f	Fraction of NPP allocated to a given biomass pool.
$k_{x,y}$	Rate of decomposition of C pool x to C pool y.
N_{up}	N uptake by plants gN m^{-2} d^{-1}.

Subscripts denoting various C pools.

cr	Coarse root biomass.
fr	Fine root biomass.
l	Foliage biomass.
w	Wood biomass.
cd	Coarse woody litter.
ssd	Surface structural litter.
fsd	Soil structural litter.
smd	Surface metabolic.
fmd	Soil metabolic.
sm	Surface microbial.
m	Soil microbial.
p	Passive.
s	Slow.
a	Released to the atmosphere.

[80] Using the C pools (biomass and soil) that are initialized using the InTEC model (Govind et al., manuscript in revision, 2009), the daily dynamics of various ecosystem C pools are modeled using BEPS-TerrainLab V2.0 using an update mechanism as described in section 2.1.2. The daily change in each C pool is a function of unique decomposition rates (as a function of seasonal variations in abiotic factors) and the corresponding C pool sizes in the previous time step.

[81] Daily change in woody biomass C pool:

$$\Delta C_{w_i} = f_w.NPP_i - k_{w,cd}.C_{w_{i-1}} \tag{B1}$$

[82] Daily change in coarse root biomass C pool:

$$\Delta C_{cr_i} = f_{cr}.NPP_i - k_{cr,cd}C_{cr_{i-1}} \tag{B2}$$

[83] Daily change in foliar biomass C pool:

$$\Delta C_{l_i} = f_l.NPP_i - k_{l,ssd}.C_{l_{i-1}} \tag{B3}$$

[84] Daily change in fine root biomass C pool:

$$\Delta C_{fr_i} = f_{fr}.NPP_i - k_{fr,fsd}.C_{fr_{i-1}} \tag{B4}$$

[85] Daily change in coarse woody litter C pool:

$$\Delta C_{cd_i} = \left[\frac{\left(k_{w,cd}.C_{w_{i-1}} + k_{cr,cd}.C_{cr_{i-1}}\right) - \left[C_{cd_{i-1}}.\left(k_{cd,a} + k_{cd,m} + k_{cd,s}\right)\right]}{\left(1 + \left(k_{cd,a} + k_{cd,m} + k_{cd,s}\right)\right)}\right] \tag{B5}$$

[86] Daily change in surface structural litter C pool:

$$\Delta C_{ssd_i} = \left[\frac{(1 - F_{m_i}).k_{l,ssd}.C_{l_{i-1}} - \left(C_{ssd_{i-1}}.\left(k_{ssd,a} + k_{ssd,sm} + k_{ssd,s}\right)\right)}{\left(1 + \left(k_{ssd,a} + k_{ssd,sm} + k_{ssd,s}\right)\right)}\right] \tag{B6}$$

[87] Daily change in surface metabolic litter C pool:

$$\Delta C_{smd_i} = \left[\frac{F_{mi}.k_{l,ssd}.C_{l_{i-1}} - \left(C_{smd_{i-1}}.\left(k_{smd,a} + k_{smd,sm}\right)\right)}{1 + \left(k_{smd,a} + k_{smd,sm}\right)}\right] \tag{B7}$$

[88] Daily change in soil structural litter C pool:

$$\Delta C_{fsd_i} = \left[\frac{(1 - F_{m_i}).k_{fr,fsd}.C_{fr_{i-1}} - \left(C_{fsd_{i-1}}.\left(k_{fsd,a} + k_{fsd,m} + k_{fsd,s}\right)\right)}{1 + \left(k_{fsd,a} + k_{fsd,m} + k_{fsd,s}\right)}\right]. \tag{B8}$$

[89] Daily change in soil metabolic litter C pool:

$$\Delta C_{fmd_i} = \left[\frac{F_{m_i}.k_{fr,fsd}.C_{fr_{i-1}} - \left(C_{fmd_{i-1}}.\left(k_{fmd,a} + k_{fmd,m}\right)\right)}{1 + \left(k_{fmd,a} + k_{fmd,m}\right)}\right]. \tag{B9}$$

[90] Daily change in surface microbial C pool:

$$\Delta C_{sm_i} = \left(C_{ssd_i}.k_{ssd,sm} + C_{smd_i}.k_{smd,sm}\right) - \left(C_{sm_{i-1}}.\left(k_{sm,a} + k_{sm,s}\right)\right). \tag{B10}$$

[91] Daily change in soil microbial C pool:

$$\Delta C_{m_i} = \left[\left(k_{fsd,m}.C_{fsd_i} + k_{fmd,m}.C_{fmd_i} + C_{cd_i}.k_{cd,m}\right) + \left(C_{s_{i-1}}.k_{s,m} + C_{p_{i-1}}.k_{p,m}\right)\right] - \left[C_{m_{i-1}}.\left(k_{m,a} + k_{m,s} + k_{m,p}\right)\right] \tag{B11}$$

[92] Daily change in slow soil C pool:

$$\Delta C_{s_i} = \left[\left(C_{m_i}.k_{m,s} + C_{cd_i}.k_{cd,s} + C_{fsdi}.k_{fsd,s}\right) + \left(C_{sm_i}.k_{sm,s} + C_{ssd_i}.k_{ssd,s}\right)\right] - \left[C_{s_{i-1}}.\left(k_{s,a} + k_{s,p} + k_{s,m}\right)\right] \tag{B12}$$

[93] Daily change in passive soil C pool:

$$\Delta C_{p_i} = \left(k_{m,p}.C_{m_i} + k_{s,p}.C_{s_i}\right) - \left(k_{p,m}.C_{p_{i-1}} + k_{p,a}.C_{p_{i-1}}\right) \quad \text{(B13)}$$

Appendix C: Soil Nitrogen Dynamics

[94] N mineralization or immobilization is simulated on the basis of the dynamics of various soil C pools and the corresponding C:N ratios. The dynamics of C:N ratios are calculated as follows [after *Ju et al.*, 2007]:

[95] C:N ratio of foliar biomass C pool:

$$CN_{l_i} = \frac{\left[(1-k_l).C_{l_{i-1}} + f_l.NPP_{i-1}\right]}{\left[\left(\frac{(1-k_l).C_{l_{i-1}}}{CN_{l_{i-1}}}\right) + \left(\frac{f_l}{CN_{l_{i-1}}}\right) \times \left(\frac{N_{up_i}}{\left[\frac{f_l}{CN_{l_{i-1}}}\right] + \left[\frac{f_{fr}}{CN_{fr_{i-1}}}\right] + \left[\frac{f_w + f_{cr}}{CN_{w_{i-1}}}\right]}\right)\right]} \quad \text{(C1)}$$

[96] C:N ratio of fine root biomass C pool:

$$CN_{fr_i} = \frac{\left[\left(1-k_{fr}\right).C_{fr_{i-1}} + f_{fr}.NPP_{i-1}\right]}{\left[\left(\frac{\left(1-k_{fr}\right).C_{fr_{i-1}}}{CNfr_{i-1}}\right) + \left(\frac{f_{fr}}{CNfr_{i-1}}\right) \times \left(\frac{N_{up_i}}{\left[\frac{f_l}{CN_{l_{i-1}}}\right] + \left[\frac{f_{fr}}{CN_{fr_{i-1}}}\right] + \left[\frac{f_w + f_{cr}}{CN_{w_{i-1}}}\right]}\right)\right]} \quad \text{(C2)}$$

[97] C:N ratio of wood and coarse root biomass C pools:

$$CN_{w/cr_i} = \frac{\left[C_{w_{i-1}} + C_{cr_{i-1}} + (f_w + f_{cr}).NPP_{i-1}\right]}{\left[\left(\frac{C_{w_{i-1}} + C_{cr_{i-1}}}{CNw_{i-1}}\right) + \left(\frac{f_w + f_{cr}}{CNw_{i-1}}\right) \times \left(\frac{N_{up_i}}{\left[\frac{f_l}{CN_{l_{i-1}}}\right] + \left[\frac{f_{fr}}{CN_{fr_{i-1}}}\right] + \left[\frac{f_w + f_{cr}}{CN_{w_{i-1}}}\right]}\right)\right]} \quad \text{(C3)}$$

[98] C:N ratio of coarse woody litter soil C pool:

$$CN_{cd_i} = \frac{C_{cd_i}}{\left[\left(\frac{C_{cd_{i-1}}}{CN_{cd_{i-1}}}\right) + \left(\frac{k_{w,cd}.C_{w_i} + k_{cr,cd}.C_{cr_i}}{CN_{w_i}}\right) - \left(\frac{C_{cd_{i-1}}\left(k_{cd,m} + k_{cd,s} + k_{cd,a}\right)}{CN_{cd_{i-1}}}\right)\right]} \quad \text{(C4)}$$

[99] C:N ratio of surface structural soil C pool:

$$CN_{ssd_i} = \frac{C_{ssd_i}}{\left[\left(\frac{C_{ssd_{i-1}}}{CN_{ssd_{i-1}}}\right) + \left(\frac{k_l.C_{l_i}\left(1-F_{m_i}\right)}{CN_{l_i}}\right) - \left(\frac{C_{ssd_{i-1}}\left(k_{ssd,sm} + k_{ssd,s} + k_{ssd,a}\right)}{CN_{ssd_{i-1}}}\right)\right]} \quad \text{(C5)}$$

[100] C:N ratio of surface metabolic soil C pool:

$$CN_{smd_i} = \frac{C_{smd_i}}{\left[\left(\frac{C_{smd_{i-1}}}{CN_{smd_{i-1}}}\right) + \left(\frac{k_l.C_{l_i}.F_{m_i}}{CN_{l_i}}\right) - \left(\frac{C_{smd_{i-1}}\left(k_{smd,sm} + k_{smd,a}\right)}{CN_{smd_{i-1}}}\right)\right]} \quad \text{(C6)}$$

[101] C:N ratio of soil structural litter soil C pool:

$$CN_{fsd_i} = \frac{C_{fsd_i}}{\left[\left(\frac{C_{fsd_{i-1}}}{CN_{fsd_{i-1}}}\right) + \left(\frac{k_{fr}.C_{fr_i}.\left(1-F_{m_i}\right)}{CN_{fr_i}}\right) - \left(\frac{C_{fsd_{i-1}}\left(k_{fsd,m} + k_{fsd,s} + k_{fsd,a}\right)}{CN_{fsd_{i-1}}}\right)\right]} \quad \text{(C7)}$$

[102] C:N ratio of soil metabolic C pool:

$$CN_{fmd_i} = \frac{C_{fmd_i}}{\left[\left(\frac{C_{fmd_{i-1}}}{CN_{fmd_{i-1}}}\right) + \left(\frac{k_{fr}.C_{fr_i}.F_{m_i}}{CN_{fr_i}}\right) - \left(\frac{C_{fmd_{i-1}}\left(k_{fmd,m} + k_{fmd,a}\right)}{CN_{fmd_{i-1}}}\right)\right]} \quad \text{(C8)}$$

[103] C:N ratio of slow soil C pool:

$$CN_{s_i} = \frac{C_{s_i}}{\left[\begin{array}{l} \left(\frac{C_{s_{i-1}}}{CN_{s_{i-1}}}\right) + \left(\frac{k_{ssd,s}.C_{ssd_{i-1}}}{CN_{ssd_i}}\right) + \left(\frac{k_{fsd,s}.C_{fsd_{i-1}}}{CN_{fsd_i}}\right) + \\ \left(\frac{k_{cd,s}.C_{cd_{i-1}}}{CN_{cd_i}}\right) + \left(\frac{k_{m,s}.C_{m_{i-1}}}{CN_{m_i}}\right) + \left(\frac{k_{sm,s}.C_{sm_{i-1}}}{CN_{sm_i}}\right) + \\ \left(\frac{C_{s_{i-1}}.\left(k_{s,m} + k_{s,p} + k_{s,a}\right)}{CN_{s_{i-1}}}\right) \end{array}\right]} \quad \text{(C9)}$$

[104] C:N ratio of passive soil C pool:

$$CN_{p_i} = \frac{C_{p_i}}{\left[\left(\frac{C_{p_{i-1}}}{CN_{p_{i-1}}}\right) + \left(\frac{k_{s,p}.C_{s_{i-1}}}{CN_{s_{i-1}}}\right) + \left(\frac{k_{m,p}.C_{m_{i-1}}}{12.0}\right) - \left(\frac{Cp_{i-1}.\left(k_{p,m} + k_{p,a}\right)}{CN_{p_{i-1}}}\right)\right]} \quad \text{(C10)}$$

[105] F_{m_i} is the partitioning fraction of leaf and fine root pools to metabolic C pool. We assume a constant C:N ratio for the microbial C pools as 1:12 because they are living beings. The dynamic nature of C:N ratios vis-à-vis the C pool sizes facilitate the calculation of N mineralization or N immobilization and therefore, the net N mineralization (sum of mineralization and immobilization) as shown in equation (C11). The positive terms are N mineralization, and negative terms are N immobilization processes.

$$\begin{aligned} N_{\min_i} = & \left[\frac{\left(k_{cd,a} + k_{cd,m} + k_{cd,s}\right).C_{cd_i}}{CN_{cd_i}}\right] \\ & + \left[\frac{\left(k_{ssd,sm} + k_{ssd,s} + k_{ssd,a}\right).C_{ssd_i}}{CN_{ssd_i}}\right] \\ & + \left[\frac{\left(k_{smd,sm} + k_{smd,a}\right).C_{smd_i}}{CN_{smd_i}}\right] \\ & + \left[\frac{\left(k_{fsd,m} + k_{fsd,s} + k_{fsd,a}\right).C_{fsd_i}}{CN_{fsd_i}}\right] \\ & + \left[\frac{\left(k_{fmd,m} + k_{fmd,a}\right).C_{fmd_i}}{CN_{fmd_i}}\right] + \left[\frac{\left(k_{sm,s} + K_{sm,a}\right).C_{sm_i}}{CN_{sm_i}}\right] \\ & + \left[\frac{\left(k_{m,s} + k_{m,p} + k_{m,a}\right).C_{m_i}}{CN_{m_i}}\right] + \left[\frac{\left(k_{s,m} + k_{s,p} + k_{s,a}\right).C_{s_i}}{CN_{s_i}}\right] \\ & + \left[\frac{\left(k_{p,m} + k_{p,s} + k_{p,a}\right).C_{p_i}}{CN_{p_i}}\right] \end{aligned}$$

$$
\begin{aligned}
&- \left[\frac{\left(k_{ssd,sm}.C_{ssd_i}\right) + \left(k_{smd,sm}.C_{smd,sm_i}\right)}{CN_{sm_i}}\right] \\
&- \left[\frac{\left(k_{s,p}.C_{s_i}\right) + \left(k_{m,p}.C_{m_i}\right)}{CN_{p_i}}\right] \\
&- \left[\frac{\left(k_{fsd,m}.C_{fsd_i}\right) + \left(k_{fmd,m}.C_{fmd_i}\right) + \left(k_{cd,m}.C_{cd_i}\right) + \left(k_{s,m}.C_{s_i}\right) + \left(k_{p,m}.C_{p_i}\right)}{CN_{m_i}}\right] \\
&- \left[\frac{\left(k_{fsd,s}.C_{fsd_i}\right) + \left(k_{fmd,s}.C_{fmd_i}\right) + \left(k_{cd,s}.C_{cd_i}\right) + \left(k_{m,s}.C_{m_i}\right) + \left(k_{p,s}.C_{p_i}\right)}{CN_{s_i}}\right] \qquad \text{(C11)}
\end{aligned}
$$

[106] **Acknowledgments.** This work was supported by the Canadian Carbon Program (CCP), funded by the Canadian Foundation for Climate and Atmospheric Sciences (CFCAS), Natural Sciences and Engineering Research Council of Canada (NSERC), and BIOCAP Canada. We thank André Beaudoin and Luc Guindon of the Laurentian Forestry Centre, Canada, for providing the land cover map, originating from the Earth Observation for Sustainable Development of Forests (EOSD) project. We thank Hank Margolis, principal investigator of CCP and the site principal investigator of the EOBS site. Oliver Sonnentag, University of California, Berkeley, is acknowledged for fruitful discussions during the course of this research work. We also thank Onil Bergeron and Carole Coursolle for their efforts in processing the flux and meteorological data sets at the EOBS.

References

Aitkenhead-Peterson, J. A., R. P. Smart, M. J. Aitkenhead, M. S. Cresser, and W. H. McDowell (2007), Spatial and temporal variation of dissolved organic carbon export from gauged and ungauged watersheds of Dee Valley, Scotland: Effect of land cover and C:N, *Water Resour. Res.*, *43*, W05442, doi:10.1029/2006WR004999.

Amiro, B. D., et al. (2006), Carbon, energy and water fluxes at mature and disturbed forest sites, Saskatchewan, Canada, *Agric. For. Meteorol.*, *136*, 237–251, doi:10.1016/j.agrformet.2004.11.012.

Arain, M. A., F. M. Yuan, and T. A. Black (2006), Soil-plant nitrogen cycling modulated carbon exchanges in a western temperate conifer forest in Canada, *Agric. For. Meteorol.*, *140*, 171–192, doi:10.1016/j.agrformet.2006.03.021.

Baldocchi, D. (2008), Breathing of the terrestrial biosphere: Lessons learned from a global network of carbon dioxide flux measurement systems, *Aust. J. Bot.*, *56*, 1–26, doi:10.1071/BT07151.

Band, L. E., P. Patterson, R. Nemani, and S. W. Running (1993), Forest ecosystem processes at the watershed scale: Incorporating hillslope hydrology, *Agric. For. Meteorol.*, *63*, 93–126, doi:10.1016/0168-1923(93)90024-C.

Band, L. E., C. L. Tague, P. Groffman, and K. Belt (2001), Forest ecosystem processes at the watershed scale: Hydrological and ecological controls of nitrogen export, *Hydrol. Process.*, *15*, 2013–2028, doi:10.1002/hyp.253.

Barr, A. G., T. A. Black, E. H. Hogg, N. Kljun, K. Morgenstern, and Z. Nesic (2004), Inter-annual variability in the leaf area index of a boreal aspen-hazelnut forest in relation to net ecosystem production, *Agric. For. Meteorol.*, *126*, 237–255, doi:10.1016/j.agrformet.2004.06.011.

Bergeron, O., H. A. Margolis, T. A. Black, C. Coursolle, A. L. Dunn, A. G. Barr, and S. C. Wofsy (2007), Comparison of carbon dioxide fluxes over three boreal black spruce forests in Canada, *Global Change Biol.*, *13*, 89–107, doi:10.1111/j.1365-2486.2006.01281.x.

Bergeron, O., H. A. Margolis, C. Coursolle, and M. A. Giasson (2008), How does forest harvest influence carbon dioxide fluxes of black spruce ecosystems in eastern North America?, *Agric. For. Meteorol.*, *148*, 537–548.

Beringer, J., A. H. Lynch, F. S. Chapin, M. Mack, and G. B. Bonan (2001), The representation of Arctic soils in the land surface model: The importance of mosses, *J. Clim.*, *14*, 3324–3335, doi:10.1175/1520-0442(2001)014<3324:TROASI>2.0.CO;2.

Beringer, J., F. S. Chapin, C. C. Thompson, and A. D. Mcguire (2005), Surface energy exchanges along a tundra-forest transition and feedbacks to climate, *Agric. For. Meteorol.*, *131*, 143–161, doi:10.1016/j.agrformet.2005.05.006.

Betts, R. A., et al. (2007), Projected increase in continental runoff due to plant responses to increasing carbon dioxide, *Nature*, *448*, 1037–1041, doi:10.1038/nature06045.

Black, T. A., D. Gaumont-Guay, R. S. Jassal, B. D. Amiro, P. G. Jarvis, S. T. Gower, F. M. Kelliher, A. Dunn, and S. C. Wofsy (2005), Measurement of CO_2 exchange between boreal forest and the atmosphere, in *The Carbon Balance of Forest Biomes*, edited by H. Griffiths and P. J. Jarvis, pp. 151–186, Taylor and Francis Group, New York.

Blodau, C., N. T. Roulet, T. Heitmann, H. Stewart, J. Beer, P. Lafleur, and T. R. Moore (2007), Belowground carbon turnover in a temperate ombrotrophic bog, *Global Biogeochem. Cycles*, *21*, GB1021, doi:10.1029/2005GB002659.

Bonan, G. B. (1995), Land atmosphere CO_2 exchange simulated by a land surface process model coupled to an atmospheric general circulation model, *J. Geophys. Res.*, *100*, 2817–2831, doi:10.1029/94JD02961.

Bond-Lamberty, B., C. K. Wang, and S. T. Gower (2004), Net primary production and net ecosystem production of a boreal black spruce wildfire chronosequence, *Global Change Biol.*, *10*, 473–487, doi:10.1111/j.1529-8817.2003.0742.x.

Bond-Lamberty, B., S. T. Gower, and D. E. Ahl (2007), Improved simulation of poorly drained forests using biome-BGC, *Tree Physiol.*, *27*, 703–715.

Boone, R. D., K. J. Nadelhoffer, J. D. Canary, and J. P. Kaye (1998), Roots exert a strong influence on the temperature sensitivity of soil respiration, *Nature*, *396*, 570–572, doi:10.1038/25119.

Byrne, K. A., G. Kiely, and P. Leahy (2007), Carbon sequestration determined using farm scale carbon balance and eddy covariance, *Agric. Ecosyst. Environ.*, *121*, 357–364, doi:10.1016/j.agee.2006.11.015.

Chen, J. M., J. Liu, J. Cihlar, and M. L. Goulden (1999), Daily canopy photosynthesis model through temporal and spatial scaling for remote sensing applications, *Ecol. Modell.*, *124*, 99–119, doi:10.1016/S0304-3800(99)00156-8.

Chen, J. M., W. M. Ju, J. Cihlar, D. Price, J. Liu, W. J. Chen, J. J. Pan, A. Black, and A. Barr (2003), Spatial distribution of carbon sources and sinks in Canada's forests, *Tellus, Ser. B*, *55*, 622–641, doi:10.1034/j.1600-0889.2003.00036.x.

Chen, J. M., X. Y. Chen, W. M. Ju, and X. Y. Geng (2005), Distributed hydrological model for mapping evapotranspiration using remote sensing inputs, *J. Hydrol.*, *305*, 15–39, doi:10.1016/j.jhydrol.2004.08.029.

Chen, J. M., A. Govind, O. Sonnentag, Y. Q. Zhang, A. Barr, and B. Amiro (2006), Leaf area index measurements at Fluxnet-Canada forest sites, *Agric. For. Meteorol.*, *140*, 257–268, doi:10.1016/j.agrformet.2006.08.005.

Chen, W. J., J. Chen, and J. Cihlar (2000), An integrated terrestrial ecosystem carbon-budget model based on changes in disturbance, climate, and atmospheric chemistry, *Ecol. Modell.*, *135*, 55–79, doi:10.1016/S0304-3800(00)00371-9.

Chen, X. F., J. M. Chen, S. Q. An, and W. M. Ju (2007), Effects of topography on simulated net primary productivity at landscape scale: Carbon sequestration in China's forest ecosystems, *J. Environ. Manage.*, *85*, 585–596, doi:10.1016/j.jenvman.2006.04.026.

Coops, N. C., T. A. Black, R. P. S. Jassal, J. A. T. Trofymow, and K. Morgenstern (2007), Comparison of MODIS, eddy covariance determined and physiologically modelled gross primary production (GPP) in a Douglas-fir forest stand, *Remote Sens. Environ.*, *107*, 385–401, doi:10.1016/j.rse.2006.09.010.

Cox, P. M., R. A. Betts, C. D. Jones, S. A. Spall, and I. J. Totterdell (2000), Acceleration of global warming due to carbon-cycle feedbacks in a coupled climate model (vol. 408, 184–187, doi:10.1038/35041539, 2000), *Nature*, *408*, 750, doi:10.1038/35047138.

Creed, I. F., and L. E. Band (1998), Exploring functional similarity in the export of nitrate-N from forested catchments: A mechanistic modeling approach, *Water Resour. Res.*, *34*, 3079–3093, doi:10.1029/98WR02102.

Daly, E., A. Porporato, and I. Rodriguez-Iturbe (2004), Coupled dynamics of photosynthesis, transpiration, and soil water balance. Part I: Upscaling from hourly to daily level, *J. Hydrometeorol.*, *5*, 546–558, doi:10.1175/1525-7541(2004)005<0546:CDOPTA>2.0.CO;2.

Dang, Q. L., H. A. Margolis, M. R. Coyea, M. Sy, and G. J. Collatz (1997), Regulation of branch-level gas exchange of boreal trees: Roles of shoot water potential and vapor pressure difference, *Tree Physiol.*, *17*, 521–535.

Davidson, E. A., and I. A. Janssens (2006), Temperature sensitivity of soil carbon decomposition and feedbacks to climate change, *Nature*, *440*, 165–173, doi:10.1038/nature04514.

Deming, D. (1995), Climatic warming in North America: Analysis of borehole temperatures, *Science*, *268*, 1576–1577, doi:10.1126/science.268.5217.1576.

Devito, K. J., C. J. Westbrook, and S. L. Schiff (1999), Nitrogen mineralization and nitrification in upland and peatland forest soils in two Canadian shield catchments, *Can. J. For. Res.*, *29*, 1793–1804, doi:10.1139/cjfr-29-11-1793.

Dietrich, W. E., and J. T. Perron (2006), The search for a topographic signature of life, *Nature*, *439*, 411–418, doi:10.1038/nature04452.

Dragoni, D., H. P. Schmid, C. S. B. Grimmond, and H. W. Loescher (2007), Uncertainty of annual net ecosystem productivity estimated using eddy covariance flux measurements, *J. Geophys. Res.*, *112*, D17102, doi:10.1029/2006JD008149.

Else, M. A., A. E. Tiekstra, S. J. Croker, W. J. Davies, and M. B. Jackson (1996), Stomatal closure in flooded tomato plants involved abscisic acid and a chemically unidentified antitranspirant in xylem sap, *Plant Physiol.*, *112*, 239–247.

Farquhar, G. D., S. V. Caemmerer, and J. A. Berry (1980), A biochemical model of photosynthetic CO_2 assimilation in leaves of C_3 species, *Planta*, *149*, 78–90, doi:10.1007/BF00386231.

Ford, D. J., W. R. Cookson, M. A. Adams, and P. F. Grierson (2007), Role of soil drying in nitrogen mineralization and microbial community function in semi-arid grasslands of north–west Australia, *Soil Biol. Biochem.*, *39*, 1557–1569, doi:10.1016/j.soilbio.2007.01.014.

Fraser, C. J. D., N. T. Roulet, and T. R. Moore (2001), Hydrology and dissolved organic carbon biogeochemistry in an ombrotrophic bog, *Hydrol. Process.*, *15*, 3151–3166, doi:10.1002/hyp.322.

Frolking, S., et al. (1996), Modelling temporal variability in the carbon balance of a spruce/moss boreal forest, *Global Change Biol.*, *2*, 343–366, doi:10.1111/j.1365-2486.1996.tb00086.x.

Gedney, N., P. M. Cox, R. A. Betts, O. Boucher, C. Huntingford, and P. A. Stott (2006), Detection of a direct carbon dioxide effect in continental river runoff records, *Nature*, *439*, 835–838, doi:10.1038/nature04504.

Giasson, M. A., C. Coursolle, and H. A. Margolis (2006), Ecosystem-level CO_2 fluxes from a boreal cutover in eastern Canada before and after scarification, *Agric. For. Meteorol.*, *140*, 23–40, doi:10.1016/j.agrformet.2006.08.001.

Goulden, M. L., and P. M. Crill (1997), Automated measurements of CO_2 exchange at the moss surface of a black spruce forest, *Tree Physiol.*, *17*, 537–542.

Goulden, M. L., et al. (1998), Sensitivity of boreal forest carbon balance to soil thaw, *Science*, *279*, 214–217, doi:10.1126/science.279.5348.214.

Govind, A., J. M. Chen, H. Margolis, and P. Y. Bernier (2006), Topographically driven lateral water fluxes and their influence on carbon assimilation of a black spruce ecosystem, *EOS Trans. AGU*, *87*(52), Fall Meet. Suppl., Abstract B23E-06.

Govind, A., J. M. Chen, H. Margolis, W. Ju, O. Sonnentag, and M. A. Giasson (2009), Model description and test in a boreal ecosystem in eastern North America, *J. Hydrol.*, doi:10.1016/j.jhydrol.2009.01.006, in press.

Grant, R. F. (2004), Modeling topographic effects on net ecosystem productivity of boreal black spruce forests, *Tree Physiol.*, *24*, 1–18.

Grant, R. F., et al. (2006), Intercomparison of techniques to model water stress effects on CO_2 and energy exchange in temperate and boreal deciduous forests, *Ecol. Modell.*, *196*, 289–312.

Griffis, T. J., T. A. Black, K. Morgenstern, A. G. Barr, Z. Nesic, G. B. Drewitt, D. Gaumont-Guay, and J. H. Mccaughey (2003), Ecophysiological controls on the carbon balances of three southern boreal forests, *Agric. For. Meteorol.*, *117*, 53–71, doi:10.1016/S0168-1923(03)00023-6.

Hornberger, G. M., K. E. Bencala, and D. M. Mcknight (1994), Hydrological controls on dissolved organic carbon during snowmelt in the Snake River near Montezuma, Colorado, *Biogeochemistry*, *25*, 147–165, doi:10.1007/BF00024390.

Humphreys, E. R., T. A. Black, K. Morgenstern, T. B. Cai, G. B. Drewitt, Z. Nesic, and J. A. Trofymow (2006), Carbon dioxide fluxes in coastal Douglas-fir stands at different stages of development after clearcut harvesting, *Agric. For. Meteorol.*, *140*, 6–22, doi:10.1016/j.agrformet.2006.03.018.

Hunt, E. R., S. C. Piper, R. Nemani, C. D. Keeling, R. D. Otto, and S. W. Running (1996), Global net carbon exchange and intra-annual atmospheric CO_2 concentrations predicted by an ecosystem process model and three-dimensional atmospheric transport model, *Global Biogeochem. Cycles*, *10*, 431–456, doi:10.1029/96GB01691.

Ito, A., M. Inatomi, W. Mo, M. Lee, H. Koizumi, N. Saigusa, S. Murayama, and S. Yamamoto (2007), Examination of model-estimated ecosystem respiration using flux measurements from a cool-temperate deciduous broad-leaved forest in central Japan, *Tellus, Ser. B*, *59*, 616–624, doi:10.1111/j.1600-0889.2007.00258.x.

Jackson, R. B., J. Canadell, J. R. Ehleringer, H. A. Mooney, O. E. Sala, and E. D. Schulze (1996), A global analysis of root distributions for terrestrial biomes, *Oecologia*, *108*, 389–411, doi:10.1007/BF00333714.

Jarvis, P. G. (1976), Interpretation of variations in leaf water potential and stomatal conductance found in canopies in field, *Philos. Trans. R. Soc. London, Ser. B*, *273*, 593–610, doi:10.1098/rstb.1976.0035.

Ju, W. M., and J. M. Chen (2005), Distribution of soil carbon stocks in Canada's forests and wetlands simulated based on drainage class, topography and remotely sensed vegetation parameters, *Hydrol. Process.*, *19*, 77–94, doi:10.1002/hyp.5775.

Ju, W. M., J. M. Chen, T. A. Black, A. G. Barr, J. Liu, and B. Z. Chen (2006), Modelling multi-year coupled carbon and water fluxes in a boreal aspen forest, *Agric. For. Meteorol.*, *140*, 136–151, doi:10.1016/j.agrformet.2006.08.008.

Ju, W. M., J. M. Chen, D. Harvey, and S. Wang (2007), Future carbon balance of China's forests under climate change and increasing CO_2: Carbon sequestration in China's forest ecosystems, *J. Environ. Manage.*, *85*(3), 538–562, doi:10.1016/j.jenvman.2006.04.028.

Kergoat, L. (1998), A model for hydrological equilibrium of leaf area index on a global scale, *J. Hydrol.*, *212–213*, 268–286, doi:10.1016/S0022-1694(98)00211-X.

Kielland, K., K. Olson, R. W. Ruess, and R. D. Boone (2006), Contribution of winter processes to soil nitrogen flux in taiga forest ecosystems, *Biogeochemistry*, *81*, 349–360, doi:10.1007/s10533-006-9045-3.

Kimball, J. S., M. A. White, and S. W. Running (1997), Biome-BGC simulations of stand hydrologic processes for BOREAS, *J. Geophys. Res.*, *102*, 29,043–29,051, doi:10.1029/97JD02235.

Kirchmann, H., S. Snall, J. Eriksson, and L. Mattsson (2005), Properties and classification of soils of the Swedish long-term fertility experiments: V. Sites at Vreta Kloster and Högåsa, *Acta Agricul. Scand. B*, *55*, 98–110.

Kozlowski, T. T. (1984), *Flooding and Plant Growth*, 356 pp., Academic, San Diego, Calif.

Krishnan, P., T. A. Black, N. J. Grant, A. G. Barr, E. T. H. Hogg, R. S. Jassal, and K. Morgenstern (2006), Impact of changing soil moisture distribution on net ecosystem productivity of a boreal aspen forest during and following drought, *Agric. For. Meteorol.*, *139*, 208–223, doi:10.1016/j.agrformet.2006.07.002.

Kuchment, L. S., V. N. Demidov, and Z. P. Startseva (2006), Coupled modeling of the hydrological and carbon cycles in the soil-vegetation-atmosphere system, *J. Hydrol.*, *323*, 4–21, doi:10.1016/j.jhydrol.2005.08.011.

Lavigne, M. B., et al. (1997), Comparing nocturnal eddy covariance measurements to estimates of ecosystem respiration made by scaling chamber measurements at six coniferous boreal sites, *J. Geophys. Res.*, *102*, 28,977–28,985, doi:10.1029/97JD01173.

Lavigne, M. B., R. J. Foster, and G. Goodine (2004), Seasonal and annual changes in soil respiration in relation to soil temperature, water potential and trenching, *Tree Physiol.*, *24*, 415–424.

Letts, M. G., N. T. Roulet, N. T. Comer, M. R. Skarupa, and D. L. Verseghy (2000), Parametrization of peatland hydraulic properties for the Canadian land surface scheme, *Atmos. Ocean*, *38*, 141–160.

Leuning, R. (1990), Modelling stomatal behaviour and photosynthesis of *Eucalyptus grandis*, *Aust. J. Plant Physiol.*, *17*, 159–175.

Liu, J., J. M. Chen, J. Cihlar, and W. M. Park (1997), A process-based boreal ecosystem productivity simulator using remote sensing inputs, *Remote Sens. Environ.*, *62*, 158–175, doi:10.1016/S0034-4257(97)00089-8.

Liu, J., J. M. Chen, J. Cihlar, and W. Chen (1999), Net primary productivity distribution in the BOREAS region from a process model using satellite and surface data, *J. Geophys. Res.*, *104*, 27,735–27,754, doi:10.1029/1999JD900768.

Liu, J., J. M. Chen, J. Cihlar, and W. Chen (2002), Net primary productivity mapped for Canada at 1-km resolution, *Global Ecol. Biogeogr.*, *11*, 115–129, doi:10.1046/j.1466-822X.2002.00278.x.

Lloyd, J., and J. A. Taylor (1994), On the temperature dependence of soil respiration, *Funct. Ecol.*, *8*, 315–323, doi:10.2307/2389824.

Mackay, D. S., and L. E. Band (1997), Forest ecosystem processes at the watershed scale: Dynamic coupling of distributed hydrology and canopy growth, *Hydrol. Process.*, *11*, 1197–1217, doi:10.1002/(SICI)1099-1085(199707)11:9<1197::AID-HYP552>3.0.CO;2-W.

Mcguire, A. D., J. M. Melillo, J. T. Randerson, W. J. Parton, M. Heimann, R. A. Meier, J. S. Clein, D. W. Kicklighter, and W. Sauf (2000), Modeling the effects of snowpack on heterotrophic respiration across northern temperate and high latitude regions: Comparison with measurements of atmospheric carbon dioxide in high latitudes, *Biogeochemistry*, *48*, 91–114, doi:10.1023/A:1006286804351.

Morales, P., et al. (2005), Comparing and evaluating process-based ecosystem model predictions of carbon and water fluxes in major European forest biomes, *Global Change Biol.*, *11*, 2211–2233, doi:10.1111/j.1365-2486.2005.01036.x.

Nakane, K., T. Kohno, T. Horikoshi, and T. Nakatsubo (1997), Soil carbon cycling at a black spruce (Picea Mariana) forest stand in Saskatchewan, Canada, *J. Geophys. Res.*, *102*, 28,785–28,793, doi:10.1029/97JD02313.

Neff, J. C., and G. P. Asner (2001), Dissolved organic carbon in terrestrial ecosystems: Synthesis and a model, *Ecosystems*, *4*, 29–48, doi:10.1007/s100210000058.

Nemani, R. R., C. D. Keeling, H. Hashimoto, W. M. Jolly, S. C. Piper, C. J. Tucker, R. B. Myneni, and S. W. Running (2003), Climate-driven increases in global terrestrial net primary production from 1982 to 1999, *Science*, *300*, 1560–1563, doi:10.1126/science.1082750.

Parton, W. J., D. S. Schimel, C. V. Cole, and D. S. Ojima (1987), Analysis of factors controlling soil organic matter levels in Great Plains grasslands, *Soil Sci. Soc. Am. J.*, *51*, 1173–1179.

Paul, E. A., and F. E. Clark (1996), *Soil Microbiology and Biochemistry*, 340 pp., Academic Press, San Diego, Calif.

Pereira, J. S., and T. T. Kozlowski (1977), Variations among woody angiosperms in response to flooding, *Physiol. Plant.*, *41*, 184–192, doi:10.1111/j.1399-3054.1977.tb05555.x.

Piirainen, S., L. Finer, H. Mannerkoski, and M. Starr (2007), Carbon, nitrogen and phosphorus leaching after site preparation at a boreal forest clear-cut area, *For. Ecol. Manage.*, *243*, 10–18, doi:10.1016/j.foreco.2007.01.053.

Porporato, A., P. D'odorico, F. Laio, and I. Rodriguez-Iturbe (2003), Hydrologic controls on soil carbon and nitrogen cycles: I. Modeling scheme, *Adv. Water Resour.*, *26*, 45–58, doi:10.1016/S0309-1708(02)00094-5.

Post, W. M., J. Pastor, A. W. King, and W. R. Emanuel (1992), Aspects of the interaction between vegetation and soil under global change, *Water Air Soil Pollut.*, *64*, 345–363, doi:10.1007/BF00477110.

Potter, C. S. (1997), An ecosystem simulation model for methane production and emission from wetlands, *Global Biogeochem. Cycles*, *11*(4), 495–506, doi:10.1029/97GB02302.

Potter, C., S. Klooster, C. R. De Carvalho, V. B. Genovese, A. Torregrosa, J. Dungan, M. Bobo, and J. Coughlan (2001), Modeling seasonal and interannual variability in ecosystem carbon cycling for the Brazilian Amazon region, *J. Geophys. Res.*, *106*, 10,423–10,446, doi:10.1029/2000JD900563.

Potter, C., S. Klooster, M. Steinbach, P. Tan, V. Kumar, S. Shekhar, R. Nemani, and R. Myneni (2003), Global teleconnections of climate to terrestrial carbon flux, *J. Geophys. Res.*, *108*(D17), 4556, doi:10.1029/2002JD002979.

Rawls, W. J., D. L. Brakensiek, and K. E. Saxton (1982), Estimation of soil-water properties, *Trans. ASAE*, *25*, 1316–1320, 1328.

Reichstein, M., et al. (2003), Modeling temporal and large-scale spatial variability of soil respiration from soil water availability, temperature and vegetation productivity indices, *Global Biogeochem. Cycles*, *17*(4), 1104, doi:10.1029/2003GB002035.

Rodriguez-Iturbe, I., A. Porporato, F. Laio, and L. Ridolfi (2001), Plants in water-controlled ecosystems—Active role in hydrologic processes and response to water stress: I. Scope and general outline, *Adv. Water Resour.*, *24*, 695–705, doi:10.1016/S0309-1708(01)00004-5.

Schroter, D., V. Wolters, and P. C. De Ruiter (2003), C and N mineralisation in the decomposer food webs of a European forest transect, *Oikos*, *102*, 294–308, doi:10.1034/j.1600-0579.2003.12064.x.

Schulze, E. D., R. Leuning, and F. M. Kelliher (1995), Environmental regulation of surface conductance for evaporation from vegetation, *Plant Ecology*, *121*, 79–87, doi:10.1007/BF00044674.

Schwarzel, K., M. Renger, R. Sauerbrey, and G. Wessolek (2002), Soil physical characteristics of peat soils, *J. Plant Nutrition Soil Sci.*, *165*, 479–486, doi:10.1002/1522-2624(200208)165:4<479::AID-JPLN479>3.0.CO;2-8.

Shao, Y., and A. Henderson-Sellers (1996), Modeling soil moisture: A project for intercomparison of land surface parameterization schemes phase 2(b), *J. Geophys. Res.*, *101*, 7227–7250, doi:10.1029/95JD03275.

Sonnentag, O., J. Talbot, J. M. Chen, and N. T. Roulet (2007), Using direct and indirect measurements of leaf area index to characterize the shrub canopy in an ombrotrophic peatland, *Agric. For. Meteorol.*, *144*, 200–212, doi:10.1016/j.agrformet.2007.03.001.

Sonnentag, O., J. M. Chen, N. T. Roulet, W. Ju, and A. Govind (2008), Spatially explicit simulation of peatland hydrology and carbon dioxide exchange: Influence of mesoscale topography, *J. Geophys. Res.*, *113*, G02005, doi:10.1029/2007JG000605.

Tague, C. L., and L. E. Band (2004), RHESSys: Regional hydro-ecologic simulation system—An object-oriented approach to spatially distributed modeling of carbon, water, and nutrient cycling, *Earth Interact.*, *8*(19), 1–42, doi:10.1175/1087-3562(2004)8<1:RRHSSO>2.0.CO;2.

Tan, X., and S. X. Chang (2007), Soil compaction and forest litter amendment affect carbon and net nitrogen mineralization in a boreal forest soil, *Soil Tillage Res.*, *93*, 77–86, doi:10.1016/j.still.2006.03.017.

Thompson, M. V., J. T. Randerson, C. M. Malmstrom, and C. B. Field (1996), Change in net primary production and heterotrophic respiration: How much is necessary to sustain the terrestrial carbon sink?, *Global Biogeochem. Cycles*, *10*, 711–726, doi:10.1029/96GB01667.

Tombul, M., Z. Akyurek, and A. U. Sorman (2004), Determination of soil hydraulic properties using pedotransfer functions in a semi-arid basin, Turkey, *Hydrol. Earth Syst. Sci.*, *8*, 1200–1209.

Traore, S., L. Thiombiano, J. R. Millogo, and S. Guinko (2007), Carbon and nitrogen enhancement in cambisols and vertisols by Acacia spp. in eastern Burkina Faso: Relation to soil respiration and microbial biomass, *Appl. Soil Ecol.*, *35*, 660–669, doi:10.1016/j.apsoil.2006.09.004.

Turner, D. P., W. D. Ritts, J. M. Styles, Z. Yang, W. B. Cohen, B. E. Law, and P. E. Thornton (2006), A diagnostic carbon flux model to monitor the effects of disturbance and interannual variation in climate on regional NEP, *Tellus, Ser. B*, *58*, 476–490, doi:10.1111/j.1600-0889.2006.00221.x.

Utset, A., I. Farre, A. Martinez-Cob, and J. Cavero (2004), Comparing Penman-Monteith and Priestley-Taylor approaches as reference-evapotranspiration inputs for modeling maize water-use under Mediterranean conditions, *Agric. Water Manage.*, *66*, 205–219, doi:10.1016/j.agwat.2003.12.003.

Wang, C. K., B. Bond-Lamberty, and S. T. Gower (2003), Carbon distribution of a well- and poorly-drained black spruce fire chronosequence, *Global Change Biol.*, *9*, 1066–1079.

Wang, S., R. F. Grant, D. L. Verseghy, and T. A. Black (2001), Modelling plant carbon and nitrogen dynamics of a boreal aspen forest in class: The Canadian land surface scheme, *Ecol. Modell.*, *142*, 135–154, doi:10.1016/S0304-3800(01)00284-8.

White, M. A., F. Hoffman, W. W. Hargrove, and R. R. Nemani (2005), A global framework for monitoring phenological responses to climate change, *Geophys. Res. Lett.*, *32*, L04705, doi:10.1029/2004GL021961.

Wilson, K. B., D. D. Baldocchi, and P. J. Hanson (2001), Leaf age affects the seasonal pattern of photosynthetic capacity and net ecosystem exchange of carbon in a deciduous forest, *Plant Cell Environ.*, *24*, 571–583, doi:10.1046/j.0016-8025.2001.00706.x.

Winner, W. E., et al. (2004), Canopy carbon gain and water use: Analysis of old-growth conifers in the Pacific Northwest, *Ecosystems*, *7*, 482–497, doi:10.1007/s10021-004-0139-2.

Wohlfarht, G., M. Bahn, E. Haubner, I. Horak, W. Michaeler, K. Rottmar, U. Tappeiner, and A. Cernusca (1999), Inter-specific variation of the biochemical limitation to photosynthesis and related leaf traits of 30 species from mountain grassland ecosystems under different land use, *Plant Cell Environ.*, *22*, 1281–1296, doi:10.1046/j.1365-3040.1999.00479.x.

Yu, G. R., Q. F. Wang, and J. Zhuang (2004), Modeling the water use efficiency of soybean and maize plants Under environmental stresses: Application of a synthetic model of photosynthesis-transpiration based on stomatal behavior, *J. Plant Physiol.*, *161*, 303–318, doi:10.1078/0176-1617-00972.

Zhang, J., and W. J. Davies (1987), ABA in roots and leaves of flooded pea plants, *J. Exp. Bot.*, *38*, 649–659, doi:10.1093/jxb/38.4.649.

Zhang, Y., T. Kadota, T. Ohata, and D. Oyunbaatar (2007), Environmental controls on evapotranspiration from sparse grassland in Mongolia, *Hydrol. Process.*, *21*, 2016–2027, doi:10.1002/hyp.6711.

Zhao, M. S., F. A. Heinsch, R. R. Nemani, and S. W. Running (2005), Improvements of the MODIS terrestrial gross and net primary production global data set, *Remote Sens. Environ.*, *95*, 164–176, doi:10.1016/j.rse.2004.12.011.

Zhou, X. L., C. H. Peng, and Q. L. Dan (2006), Formulating and parameterizing the allocation of net primary productivity for modeling overmature stands in boreal forest ecosystems, *Ecol. Modell.*, *195*, 264–272, doi:10.1016/j.ecolmodel.2005.11.022.

Zhuang, Q., J. M. Melillo, D. W. Kicklighter, R. G. Prinn, A. D. Mcguire, P. A. Steudler, B. S. Felzer, and S. Hu (2004), Methane fluxes between terrestrial ecosystems and the atmosphere at northern high latitudes during the past century: A retrospective analysis with a process-based biogeochemistry model, *Global Biogeochem. Cycles*, *18*, GB3010, doi:10.1029/2004GB002239.

Zimov, S. A., E. A. G. Schuur, and F. S. Chapin (2006), Permafrost and the global carbon budget, *Science*, *312*, 1612–1613, doi:10.1126/science.1128908.

J. M. Chen and A. Govind, Department of Geography, University of Toronto, Sydney Smith Hall, Room 5047, 100 St. George Street, Toronto, ON M5S 3G3, Canada. (chenj@geog.utoronto.ca; ajit.govind@utoronto.ca)

W. Ju, International Institute for Earth System Sciences, Nanjing University, 22 Hanhou Road, Nanjing 210093, China. (juweimin@nju.edu.cn)